Master thesis

Supercooled Simultaneous Composite Casting for Microstructure Refinement of Alloy

Kim, Yong Ki (金容基)

Department of Ferrous Technology

(Computational Metallurgy)

Graduate Institute of Ferrous Technology

Pohang University of Science and Technology

2008

Supercooled Simultaneous Composite Casting for Microstructure Refinement of Alloy 2008 Kim, Yong Ki

다중 주조 시스템과 그로 인한 합금의 미세구조 개선 효과

Supercooled Simultaneous Composite Casting for Microstructure Refinement of Alloy

Supercooled Simultaneous Composite Casting for Microstructure Refinement of Alloy

by

Kim, Yong Ki
Department of Ferrous Technology
(Computational Metallurgy)
Graduate Institute of Ferrous Technology
Pohang University of Science and Technology

A thesis submitted to the faculty of Pohang University of Science and Technology in partial fulfillments of the requirements for the degree of Master of Science in the Graduate Institute of Ferrous Technology (Computational Metallurgy)

Pohang, Korea
December 24th, 2008

Approved by

Prof. Bhadeshia, H.K.D.H.
Major Advisor

Prof. Qin, Rongshan
Co-Advisor

Supercooled Simultaneous Composite Casting for Microstructure Refinement of Alloy

Kim, Yong Ki

This dissertation is submitted for the degree of Master of Science at the Graduate Institute of Ferrous Technology of Pohang University of Science and Technology. The research reported herein was approved by the committee of Thesis Appraisal

December 19th, 2008

Thesis Review Committee

Chairman: Prof. Lee, Hae Geon

(Signature)_____

Member: Prof. Qin, Rong Shan

(Signature)_____

Member: Prof. Kim. In Gee

(Signature)_____

MFT 20072854
Kim, Yong Ki
Supercooled Simultaneous Composite Casting for Microstructure Refinement of Alloy, Department of Ferrous Technology (Computational Metallurgy) 2007
Advisor: Prof. Bhadeshia, H.K.D.H.; Prof. Qin, Rongshan;
Text in English

Abstract

The objective of this work was to introduce a novel method for refining the solidification microstructure. Traditional casting usually solidifies one homogeneous liquid by removing heat from liquid surface, by which the microstructure solely depends on the heat removal rate for the given alloy composition. The newly developed multi-liquid composite simultaneous casting concept raises an alternative to control microstructure. The concept introduces the solidification while mixing technique so that the microstructure depends not only on the heat-removing from liquid surface but also the heat transfer from one liquid to another. In the present work reports the experimental validation of the concept by two-liquid casting of Sn-Pb alloys. Reduced grain size, increased microhardness, rougher and more fractal grain surfaces are observed for the alloy solidified by two-liquid casting in comparison of the microstructure obtained by conventional solidification techniques.

Contents

Abstract…… i

Contents……..…….ii

Nomenclature…….……. v

Ⅰ Introduction..……..……..…..**1**

Introduction……..…….……1

1.1 Aim of the Work……..……1

1.2 Theoretical Background……..3

1.3 Heat Transfer……6

1.3.1 Conduction……..……..…6

1.3.2 Convection……6

1.3.3 Radiation……..……..7

1.4 Mass Transfer……..8

1.5 Casting……..……9

1.5.1 Centrifugal Casting……9

1.5.2 Continuous Casting……9

1.6 Nucleation...……11

1.6.1 Homogeneous Nucleation..……..11

1.6.2 Nucleation Rate…...……..15

1.6.3 Heterogeneous Nucleation……18

1.7 Grain Structure……23

1.7.1 Dendrites…… ……..……25

1.8 Hardness……..……26

1.9 Dissipative particle dynamics ……..……27

1.10 Summary…….……30

Ⅱ Experiments……...……...……...31

2.1 Alloy Production.……..……...……...31

2.2 Optical Microscopy……..33

2.3 Hardness Test……..34

2.4 Energy Dispersive Spectroscopy……...…….34

2.5 X-ray Diffraction.……34

Ⅲ Results and Discussions.....……35

3.1 Optical Microscopy……...……..……35

3.1.1 One-Liquid Casting.……...35

3.1.2 Two-Liquid Casting.…….....…..…37

3.1.3 Discussion.…….…39

3.2 Microhardness Tests……41

3.3 Energy Dispersive Spectroscopy…….…43

3.4 X-ray Diffraction.……..…55

3.5 Discussion.……...58

3.6 Summary……..…60

Ⅳ Summary and Future work……61

4.1 Summary……..61

4.2 Future work……62

References……64

Acknowledgements……68

Curriculum Vitae……69

Nomenclature

A	Surface area
A_C	Surface area of nucleus-inclusion contacting area
A_S	Surface area of the spherical cap
a	Average distance between two nearest-neighbored atom in liquid
a_{ij}	Repulsive force parameter between particle i and j
C	Weight percent composition of liquid
C_A	Weight percent composition of liquid A
C_B	Weight percent composition of liquid B
D	Diffusion coefficient, diffusivity
d	Grain diameter
$\boldsymbol{F}^C$	Conservative force
$\boldsymbol{F}^D$	Dissipative force
$\boldsymbol{F}^R$	Random force
G_S	Free energy of solid phase per volume
G_L	Free energy of liquid phase per volume
ΔG_A	Activation energy
ΔG_v	Volume free energy
ΔG^*	Critical free energy change
ΔH_f	Latent heat of fusion
J	Diffusion flux

K_1	Total number of nuclei of the solid phase
k	Thermal conductivity of the materials
k_y	Strengthening coefficient
$\bar{L}$	Mean lineal intercept
n_s	Total number of atom around the incubating agents' surface in liquid
$n*$	Number of stable nuclei at critical radius
n^*_{he},	Number of nucleus at critical radius in heterogeneous nucleation
Q	Rate of heat transfer by conduction
r	radius of atom
$r*$	critical nucleus radius
$\boldsymbol{r}_{ij}$	Distance between particle *i* and *j*
$\hat{\boldsymbol{r}}_{ij}$	Unit vector in the direction of r_{ij}
T	Melting temperature of liquid
T_A	Melting temperature of liquid A
T_B	Melting temperature of liquid B
T_m	Equilibrium solidification temperature
Δt	Integration time step
V	Volume of the nucleus
$\boldsymbol{v}_{ij}$	Relative velocities of the particle *i* and *j*
ω^C	Conservative force weight function
ω^D	Dissipative force weight function
ω^R	Random force weight function

ω^*	Number of atoms surrounding a critical nucleus
$\omega_s{}^*$	Number of atom surrounding the surface of a critical nucleus
σ	Stefan-Boltzmann constant
σ_0	Materials constant for the starting stress for dislocation movement
σ_{IL}	Interface energies of inclusion-liquid
σ_{IN}	Interface energies of inclusion-nucleus
σ_{NL}	Interface energies of nucleus-liquid
σ_{SL}	The interface energy between solid and liquid
σ_y	Yield stress
σ^R	Magnitude of the random pair force between the particles
ν_{LS}	Frequency of atom jump across the liquid-solid interface
Γ	Jump frequency of an atom in liquid
λ	Jump distance of atom in liquid.
θ	Nucleus-inclusion wetting angle
ζ	Strength of the dissipative force
ξ_{ij}	Gaussian distributed random variable

Ⅰ. Introduction

1.1 Aim of the Work

Alloys with finer structures usually have better mechanical properties at ambient temperatures, although recent work on nanocrystalline single-phase structures have shown a compromised level of ductility (He and Ma, 1996; Sevillano and Aldazabal, 2004). Nevertheless, for the more normal scales of structure, strength at low temperatures increases as the grain size is refined according to the classical Hall-petch relationship (Hall, 1951; Petch, 1953),

$$\sigma_y = \sigma_0 + \frac{k_y}{\sqrt{d}} \tag{1.1}$$

where σ_y is yield stress, σ_o is a materials constant for the starting stress for dislocation movement, k_y is the strengthening coefficient, and d is grain size.

Ever since the classical experiments on undercooled liquids (Vonnegut, 1948; Chen and Turnbull, 1967; Chen and Turnbull, 1968), there have been many attempts at exploiting the resulting supersaturation to produce refined microstructures. Among the methods available for refining structure is the rapid quenching of liquid alloys. Heat removal from melt to its environment permits a large undercooling to be

achieved before solidification commences. This method is powerful in making samples which are small in at least one of the three dimensions, but is not suitable for bulk alloys where it is impossible to remove heat sufficiently rapidly (Greer, 1995). Another technique is the addition of solutes which improve nucleation capability. The added elements can act as nucleation agents but can also modify the solid-liquid interface energy in a way which results in a reduced nucleation barrier. However, the technology for doing this is difficult, particularly in introducing the distribution of nucleants in a uniform manner (Flemings, 1974). Stirring is another method for improving the solidification process. This can be done mechanically or electromagnetically with the aim of breaking dendrites in the semi-solid state. The resulting fragments provide new growth centres resulting in a finer microstructure (Fan, 2002; Campanella et al., 2004). External fields such as radiation or electric field can alter thermodynamic properties such as the driving force for the liquid-solid phase transition (Qin and Zhou, 1998).

The aim of the present work was to introduce a novel method for refining the solidification microstructure. It involves the simultaneous casting of several liquid streams which have different liquidus temperatures and chemical compositions. The technique should result in one liquid constitutionally supercooling the other with obvious consequences on the microstructure.

1.2 Theoretical Background

Conventional one-liquid casting involves a homogeneous composition and temperature, Fig. 1.1. The liquid, which has a melting temperature T and composition C is poured into a mould. Heat removal then occurs between the interface of mould wall and liquid.

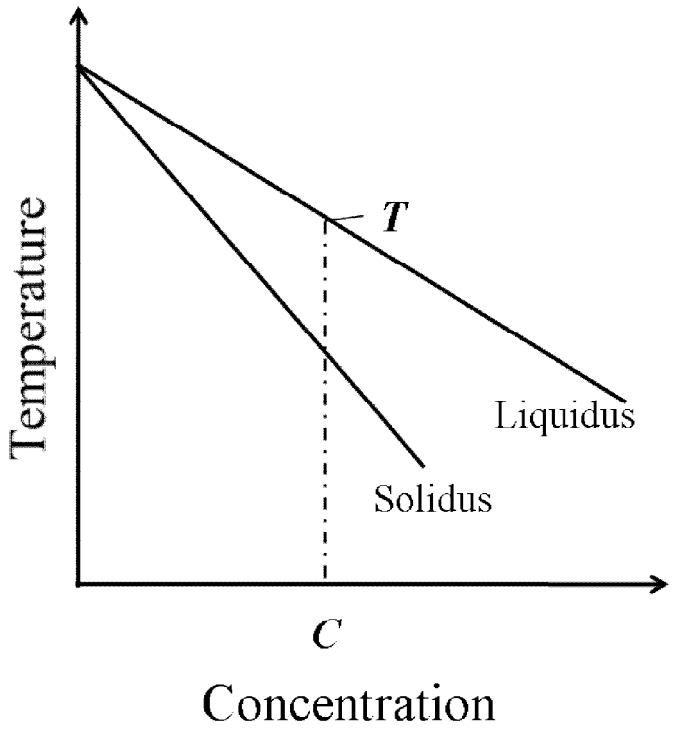

Fig. 1.1: schematic illustration of phase diagram relevant to one-liquid conventional casting. T is liquidus temperature of when concentration is C.

A large supercooling can in principle be achieved by increasing the heat removal rate while preventing heterogeneous nucleation. However, the latter is difficult to avoid when dealing with the large scale production of alloys because of unavoidable inclusions, mould walls etc. In one-liquid casting, the main technique of refining microstructure is rapid quenching, which has proved powerful in producing large supercoolings in samples which are thin in at least one dimension (Beckermann, 1993). As pointed out earlier, this is not suitable for the production of bulk alloys.

It is proposed in the present work that the simultaneous casting of two alloys, as illustrated in Fig. 1.2 is a practical method of achieving undercooling in large melts. The method involves mixing during the solidification of two liquids. Liquid A which has composition C_A and melting temperature T_A and Liquid B which has composition C_B and melting temperature T_B are cast simultaneously to achieve the desired mean composition *C*.

The vigorous flow during liquid pouring and strong convection in the mold should help liquids break into small droplets or layers dispersed throughout the melt. When layers of different liquid phases come into contact, heat transfers from the high temperature liquid layers into those of the low temperature liquid, driven by the temperature difference. Solute may also partition between the liquids. In the high temperature liquid, heat transfer lowers its temperature but solute enrichment decreases its solidus temperature. Given that heat conductivity is orders of magnitude larger than solute diffusivity, this results in the high temperature liquid

being supercooled.

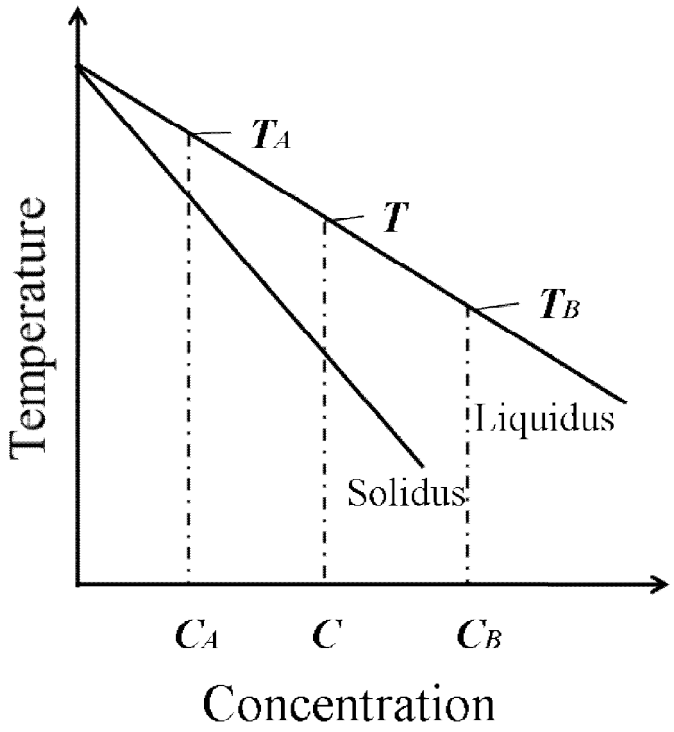

Fig. 1.2: schematic illustration of phase diagram relevant to two-liquid casting. T_A, T *and* T_B are liquidus temperatures of when concentrations are C_A, C, C_B.

The resulting nuclei are dispersed into the entire melt by fluid mixing. Heat removal happens not only at the interface of the alloy and mould wall but also between the component liquids. In these circumstances, it is possible to achieve undercooling inside the bulk of the material even in large scale applications.

1.3 Heat Transfer

1.3.1 Conduction

There are three modes of heat transfer: conduction, convection and radiation (Flemings, 1974). Conduction is the transfer of thermal energy from a region of higher temperature to one at a lower temperature through direct molecular communication without flow. Heat conduction in solids is by phonons and free electrons, in liquids by phonons, free electrons and some transitional movement of atoms, while in gases it occurs by random collisions. The one dimensional Fourier's first law is that the rate of heat transfer is assumed to be proportional to the temperature gradient,

$$Q = -kA\frac{\partial T}{\partial x} \tag{1.2}$$

where Q is the heat flux by conduction, k is the thermal conductivity of the material, A is the surface area through which heat flows.

1.3.2 Convection

Convection is one of the major modes of heat and mass transfer in liquids and gases. In casting process, liquid metal is poured into a mould for solidification. Convection

then happens because of momentum of liquid metal acquired during pouring and density difference at different part of the liquid. The former is a description of forced convection and the latter of free convection. Forced convection can be generated by external forces such as mechanical and electromagnetic stiring. In forced convection, the fluid motion is caused by an imposed pressure difference. In convection free liquid, the fluid motion arises solely due to a local buoyancy difference. The density difference can be due to the temperature or constitutional difference.

1.3.3 Radiation

Thermal radiation transports energy via electromagnetic waves. The rate of energy emission depends on the surface temperature and condition. The thermal radiation power of a black body is

$$e_b = \sigma \cdot A \cdot T^4 \tag{1.3}$$

where σ is the Stefan-Boltzmann constant and has $\sigma = 5.67 \times 10^{-8}\ W\ m^{-2}\ K^{-4}$, A is the surface area and T is the temperature.

1.4 Mass transfer

There are two modes of mass transfer, diffusion and fluid flow (Cussler, 1997). Fick's first law of diffusion describes diffusion flux in a chemically inhomogeneous domain. For a binary system the one-dimensional solute flux J is assumed to be given by

$$J = -D\frac{\partial C}{\partial x} \tag{1.4}$$

where D is the temperature dependent diffusion coefficient, C is the concentration and x is the position.

Fick's second law of diffusion describes the time-dependence of the concentration gradient and can be derived from the first law. For diffusion along one-dimension in a binary system,

$$\frac{\partial C}{\partial t} = -\frac{\partial}{\partial x}J = \frac{\partial}{\partial x}\left(D\frac{\partial C}{\partial x}\right) \tag{1.5}$$

The corresponding three-dimensional form is

$$\frac{\partial C}{\partial t} = \nabla \cdot (D\nabla C) \tag{1.6}$$

1.5 Casting

Casting is a process to make a solid shape by pouring liquid into a mould followed by solidification. There are many variants of the process such as sand casting, permanent mould casting, die casting, centrifugal casting, continuous casting, roll casting etc (Flemings, 1974).

1.5.1 Centrifugal Casting

Centrifugal casting is suited for products with an axial symmetry. Molten metal is poured into a cylindrical mould spinning about its axis of symmetry and a molten metal layer is deposited on the inside of mould wall at a uniform thickness by the centrifugal force. The mould is kept rotating until solidification is finished. This method is suitable for making products such as wheels and pipes.

1.5.2 Continuous Casting

Continuous casting is a process that can achieve high volume production of ingots with a constant cross-section, Fig. 1.3. Molten steel is poured continuously and semi-solid billet is withdrawn with continuous heat removal using cooling spray. Continuous casting is an automated process with high productivity.

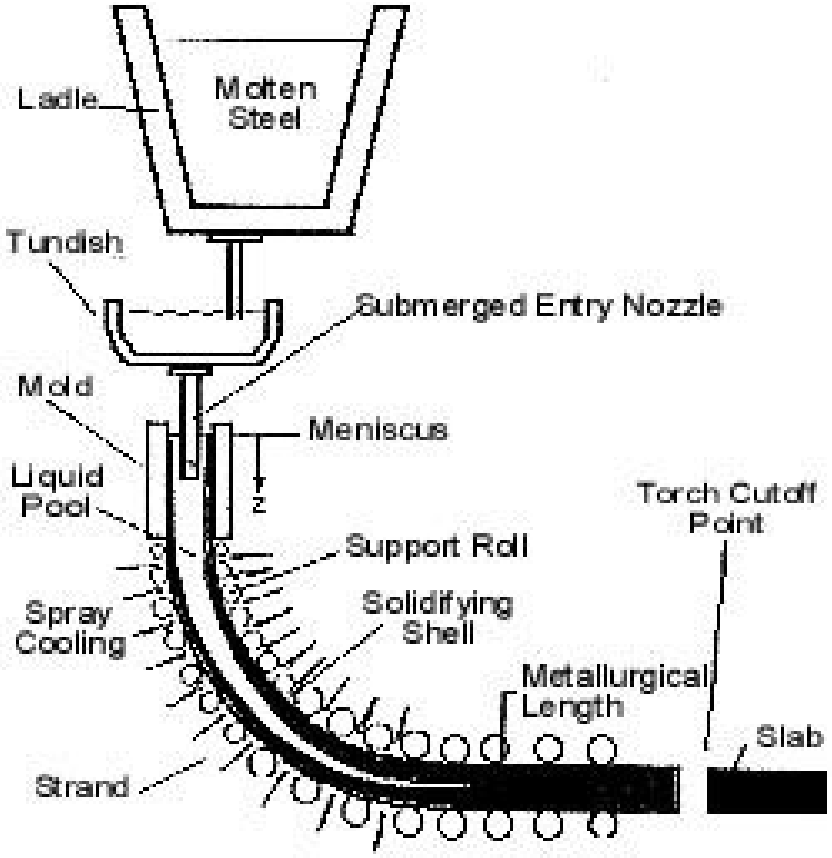

Fig. 1.3: Schematic representation of the continuous casting process

(Thomas, B. G., 1999)

1.6 Nucleation

1.6.1 Homogeneous Nucleation

There are two types of nucleation: homogeneous nucleation and heterogeneous one depending on whether the nucleus forms in isolation or in contact with a defect such as an inclusion (Flemings, 1974).

Nucleation at sites other than defects is said to be homogeneous. The free energy change consists of the free energy difference between the solid and liquid phases and the energy of the surface created between the nucleus and the parent:

$$\Delta G = G_{after} - G_{before} = V(G_S - G_L) + A\sigma_{SL} \tag{1.7}$$

where V is the volume of the nucleus, G_S and G_L are free energy of solid and liquid phases per volume, A is surface area and σ_{SL} is the interface energy between solid and liquid.

For the spherical nucleus as illustrated in Fig. 1.4:

$$\Delta G = -\frac{4\pi}{3} r^3 (G_L - G_S) + 4\pi r^2 \sigma_{SL} \tag{1.8}$$

where r is radius of the nucleus.

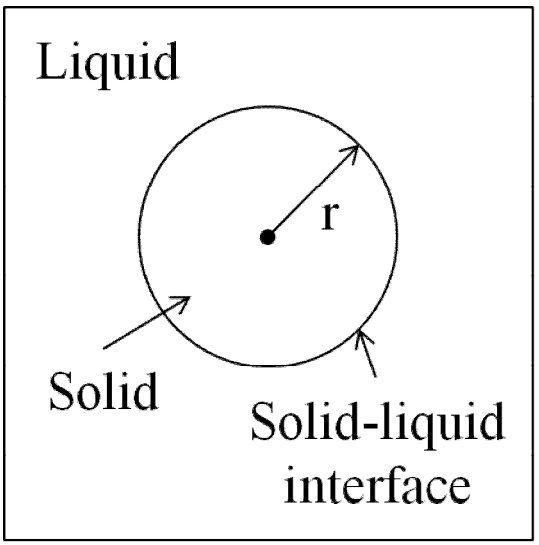

Fig. 1.4: Nucleation of a spherical solid particle in a liquid.

These volume, surface, and total energy contributions are plotted schematically as a function of nucleus radius in Fig. 1.5. The, volume free energy contribution part decreases with the third power of *r*. The surface free energy on the other hand increases with the square of the radius. Consequently the sum of the two terms passes through a maximum. ΔG achieves a maximum value ΔG^* when r=r*. The particle of radius r* is the critical nucleus, which can be obtained by setting $d\Delta G/dr = 0$.

$$r^* = \frac{2\sigma_{SL}}{(G_L - G_S)} \tag{1.9}$$

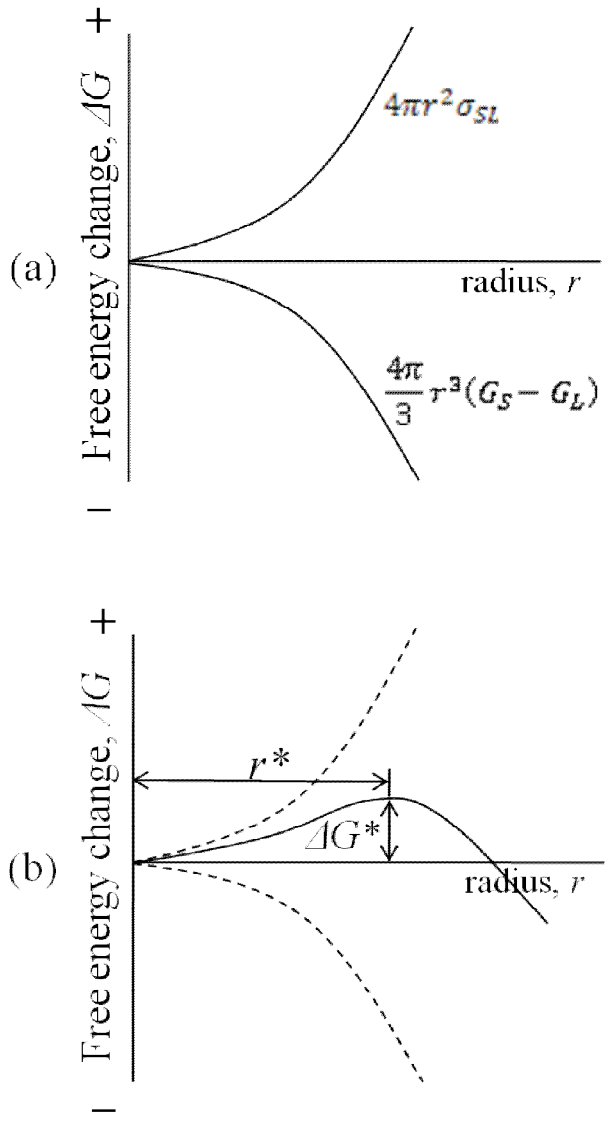

Fig. 1.5: (a) Schematic curves for volume free energy and surface free energy contributions to the total free energy change attending the formation of a spherical embryo/nucleus during solidification. (b) Schematic plot of free energy versus embryo/nucleus radius, on which in shown the critical free energy change (ΔG^*) and the critical nucleus radius (r^*).

Substitution of this expression for r^* into equation (1.8) yields:

$$\Delta G^* = \frac{16\pi {\sigma_{SL}}^3}{3(\Delta G_v)^2} \tag{1.10}$$

where $\Delta G_v (= G_S - G_L)$ is volume free energy change.

ΔG_v is a function of temperature,

$$\Delta G_v = \frac{\Delta H_f (T_m - T)}{T_m} \tag{1.11}$$

where ΔH_f is the latent heat of fusion and T_m is equilibrium solidification temperature in Kelvin. Substitution of this expression into equation (1.9) and (1.10) yields

$$r^* = \left(-\frac{2\sigma_{SL} T_m}{\Delta H_f}\right)\left(\frac{1}{T_m - T}\right) \tag{1.12}$$

and

$$\Delta G^* = \left(\frac{16\pi {\sigma_{SL}}^3 {T_m}^2}{3{\Delta H_f}^2}\right)\frac{1}{(T_m - T)^2} \tag{1.13}$$

Thus, from these two equations, both the critical radius r^* and the activation free energy ΔG^* decrease as temperature T decreases as seen in Fig. 1.6. Physically, this means that nucleation occurs more readily with a lowering of temperature below that for equilibrium solidification (T_m). Furthermore, the number of stable nuclei n^* which are having radii greater than r^* is a function of temperature as

$$n^* = K_1 \exp\left(-\frac{\Delta G^*}{kT}\right) \tag{1.14}$$

where the constant K_1 is related to the total number of nuclei of the solid phase.

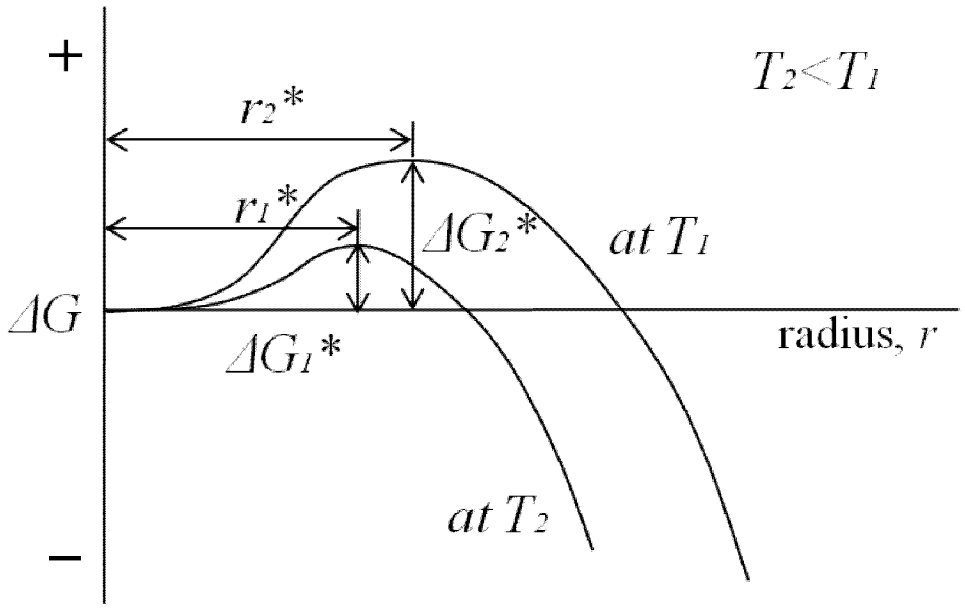

Fig. 1.6: Schematic free energy-versus-embryo/nucleus radius curves for two different temperatures. The critical free energy (ΔG^*) and critical nucleus radius (r*) are indicated for each temperature.

1.6.2 Nucleation Rate

The addition of a single atom to a critical nucleus makes that nucleus supercritical and able to grow rapidly. The nucleus rate I is given by

$$I = n_i^* \times \omega^* \times \nu_{LS} \tag{1.15}$$

where w^* is the number of atoms surrounding a critical nucleus, ν_{LS} is the frequency of atom jump across the liquid-solid interface.

For a spherical nucleus, ω^* is approximately given by

$$\omega^* = \frac{4\pi r^{*2}}{a^2} \tag{1.16}$$

where a is the average distance between two nearest-neighbored atom in liquid.

The diffusivity is given by

$$D_L = \frac{1}{6}\Gamma\lambda^2 \tag{1.17}$$

where Γ is the jump frequency of an atom in liquid and λ is the jump distance of atom in liquid. Taking $\lambda \approx a$ and considering that the atom jumping along one direction is one-sixth of all possible jump directions, it follows that

$$\nu_{SL} = \frac{D_L}{a^2} \tag{1.18}$$

Substitution equations (1.14), (1.16) and (1.18) into equation (1.15) yields

$$I = n\frac{4\pi r^{*2}}{a^4} D_L \exp\left(-\frac{\Delta G^*}{kT}\right) \tag{1.19}$$

The diffusivity D_L changes with the liquid temperature in a relationship of

$$D_L = D_0 \exp\left(-\frac{\Delta \mathrm{G_A}}{kT}\right) \tag{1.20}$$

where $\Delta \mathrm{G_A}$ is the activation energy which barely depends on temperature.

A large undercooling leads to a reduction in the nucleation rate because of sluggish diffusion. Equation (1.19) shows that when the nucleation rate approaches zero as the supercooling is reduced because $\Delta G^* \propto \frac{1}{\Delta T^2}$ which makes $\Delta G^* \to \infty$ when $\Delta T \to 0$. An increasing in supercooling will enhance the nucleation rate. The

nucleation rate will initially increase with supercooling, but it will then decrease because of the reduced mobility of atoms at low temperatures, as illustrated in Fig. 1.7.

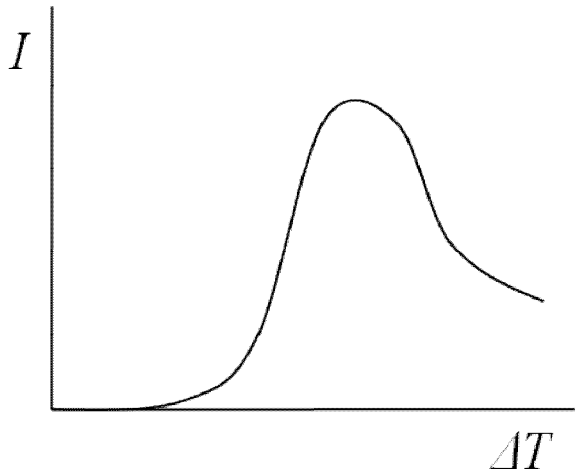

Fig. 1.7: Nucleation rate as a function of supercooling.

For many materials such as glasses and polymers, the nucleation rate and supercooling relationship agrees with Fig. 1.7. However, for the majority of metals especially pure metals, the dropping tail of nucleation rate at low temperatures has not been found (Flemings, 1974). It is established that the relationship between nucleation rate and supercooling in pure metal is more as illustrated in Fig. 1.8.

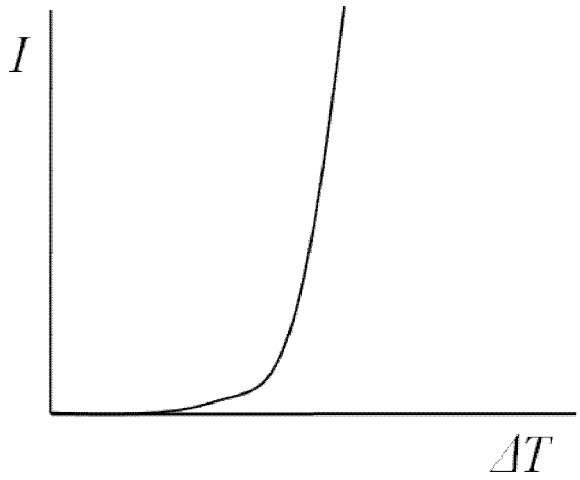

Fig. 1.8: Nucleation rate with respect to supercooling in metals.

1.6.3 Heterogeneous Nucleation

In engineering practice, many liquid metals start solidification within a few degrees of supercooling. The thermodynamic barrier for nucleation in this case is smaller than that calculated assuming homogeneous nucleation. The solidification begins on heterogeneities, e.g. inclusions, mold walls, surfaces and interfaces. To calculate the thermodynamic barrier for heterogeneous nucleation, it is necessary to consider the case illustrated in Fig. 1.9, where a spherical cap shaped nucleus is formed in a flat inclusion surface.

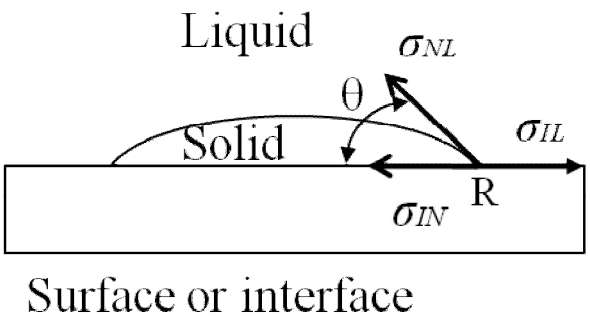

Fig. 1.9: Heterogeneous nucleation of a solid from a liquid.

For balance at position R gives

$$\sigma_{IL} = \sigma_{IN} + \sigma_{NL}cos\theta \tag{1.21}$$

where σ_{IL}, σ_{IN} and σ_{NL} are the interface energies of inclusion-liquid, inclusion-nucleus and nucleus-liquid, respectively and θ is the nucleus-inclusion wetting angle.

The nucleus is a spherical cap of radius *r*. the volume of the nucleus is given by

$$V = \frac{1}{3}\pi r^3(2 - 3cos\theta + cos^3\theta) \tag{1.22}$$

The surface are of the spherical cap is

$$A_S = 2\pi r^2(1 - cos\theta) \tag{1.23}$$

The surface area of nucleus-inclusion contact area is

$$A_C = \pi r^2 sin^2\theta = \pi r^2(1 - cos^2\theta) \tag{1.24}$$

The free energy change during the heterogeneous nucleation is

$$\Delta G_{he} = -\frac{1}{3}\pi r^3(2 - 3cos\theta + cos^3\theta)(G_L - G_S) + 2\pi r^2(1 - cos\theta)\sigma_{NL} + \pi r^2(1 - cos^2\theta)\sigma_{IN} - \pi r^2(1 - cos^2\theta)\sigma_{IL} \quad (1.25)$$

where ΔG_{he} is heterogeneous nucleation barrier. By using equation (1.21), it changes into

$$\begin{aligned}\Delta G_{he} &= -\frac{1}{3}\pi r^3(2 - 3cos\theta + cos^3\theta)(G_L - G_S) \\ &\quad + \pi r^2\sigma_{NL}(2 - 3cos\theta + cos^3\theta) \\ &= \left[-\frac{4}{3}\pi r^3(G_L - G_S) + 4\pi r^2\sigma_{NL}\right]\left(\frac{2-3cos\theta+cos^3\theta}{4}\right) \\ &= \Delta G_{ho} f(\theta) \end{aligned} \quad (1.26)$$

where ΔG_{ho} is homogeneous nucleation barrier, we defined

$$f(\theta) = \left(\frac{2-3cos\theta+cos^3\theta}{4}\right) \quad (1.27)$$

The critical radius of nucleus, *r**, is the same as defined in homogeneous nucleation.

However, the free energy to form a cap of this size on the substrate ΔG^*_{he} is smaller by a factor of $f(\theta)$.

$$\Delta G^*_{he} = \Delta G^*_{ho} f(\theta) \quad (1.28)$$

where $f(\theta)$ goes to zero as the wetting angle θ decrease to zero. This means that the nucleation barrier decreases, ultimately vanishing, as the wetting between forming particle and substrate improves. In the case of $f(\theta) = 0$ when $\theta = 0$, liquid can solidify without any supercooling. $f(\theta) = 1$ when $\theta = 180$, in which

the inclusion does not play any role and $\Delta G^*_{he} = \Delta G^*_{ho}$. The relationship between $\Delta G^*_{he}/\Delta G^*_{ho}$ and wetting angle is plotted in Fig. 1. 10.

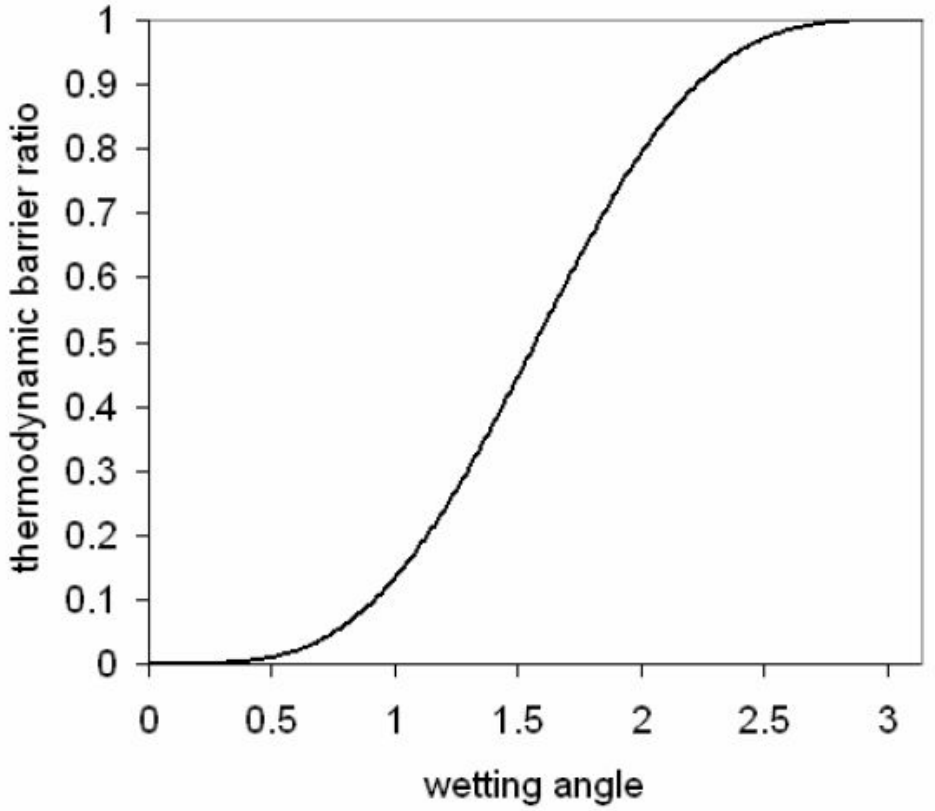

Fig. 1.10: Relation between $\Delta G^*_{he}/\Delta G^*_{ho}$ and wetting angle

The number of nuclei of critical radius, n^*_{he} can be derived in the same way as homogeneous case and takes the format

$$n^*_{he} = n_s \exp\left(-\frac{\Delta G^*_{he}}{kT}\right) \tag{1.29}$$

where n_s is the total number of atom around the incubating agents' surface in liquid.

The heterogeneous nucleation rate is given by

$$I = n_{he}{}^{*} \times \omega_{s}{}^{*} \times \nu_{LS} \tag{1.30}$$

where $\omega_{s}{}^{*}$ is the number of atom surrounding the surface of a critical nucleus and ν_{LS} is the atom jumping frequency. The relationship between nucleus rate of liquid metals and supercooling is illustrated schematically in Fig 1.11.

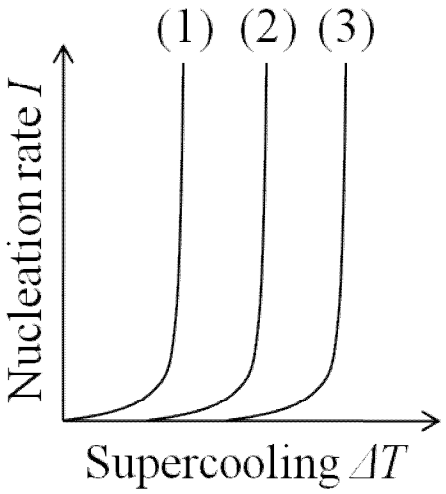

Fig 1.11: Nucleation rate for (1) heterogeneous nucleation with small wetting angle, (2) heterogeneous nucleation with large wetting angle and (3) homogeneous nucleation.

Heterogeneous nucleation needs a relatively small supercooling to stimulate. The smaller the wetting angle is the smaller supercooling needed. However, heterogeneous nucleation is limited by the surface area of the inclusions and walls,

which is basically different from homogeneous nucleation where nucleation can happen at anywhere in the liquid. When the solid growth rate is large, one can assume that each inoculating particle can act as one nucleus only. The cast grain refinement can be estimated by the number of nucleation agents.

1.7 Grain Structure

The classical picture of the grain structure of a casting or ingot is shown schematically in Fig 1.12, with the outer chill zone, the intermediate columnar zone, and the central equiaxed zone (Flemings, 1974). All three of these zones are sometimes seen in castings and ingots of real materials, especially in plain carbon or low-alloy steel. More often, however, one or another of the zones is absent. In stainless steels, the structure is often fully columnar, with no central equiaxed zone and little or no chill zone. In well-refined aluminium alloys, on the other hand, the structure is fully equiaxed. The presence and extent of these zones in the ingot structures are known to depend both on nucleation and on crystal multiplication.

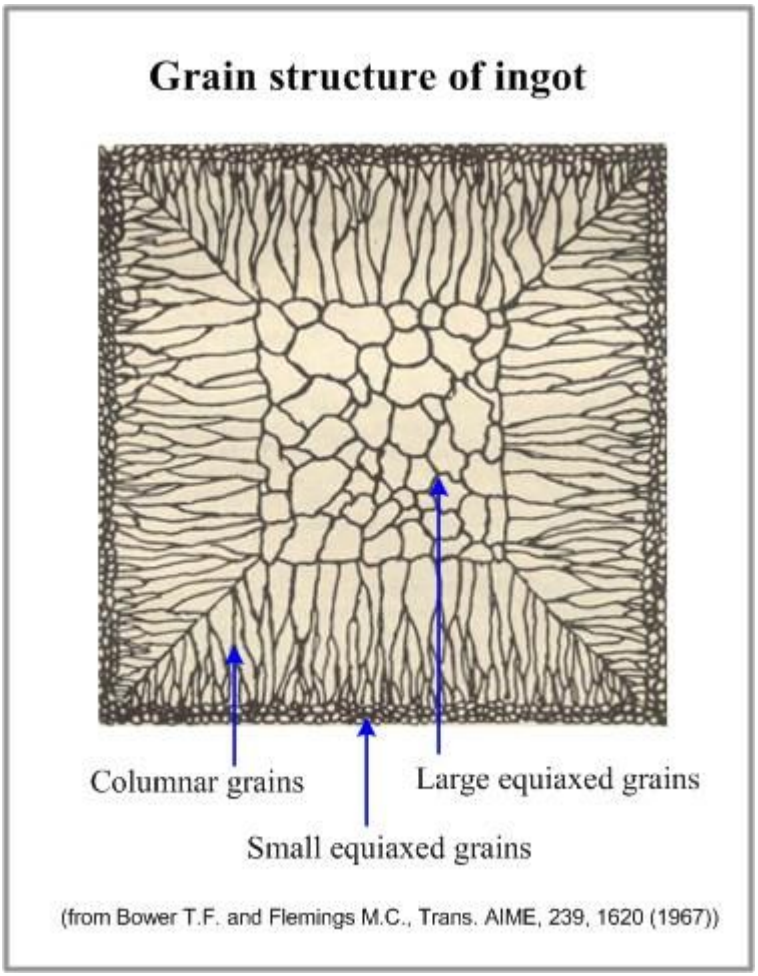

Fig 1.12: Sketch of ingot structure showing chill zone, columnar zone, equiaxed zone

1.7.1 Dendrites

When regular cells form and grow at relatively low rates, they grow normal to the liquid-solid interface regardless of crystal orientation. When, however, the growth rate is increased, crystallographic effects begin to exert an influence and the cell-growth direction deviates toward the preferred crystallographic growth direction. Simultaneously, the cross section of the cell generally begins to deviate from its previously circular geometry owing to effects of crystallography. This structure has been described variously as a flanged structure, or maltese cross, in cubic materials; it is shown in Fig. 1.13. As the growth rate increases still further, the cross structure first becomes more apparent and then serrations begin to appear in the flanges of the cross; that is, secondary dendrite arms become discernible (Flemings, 1974).

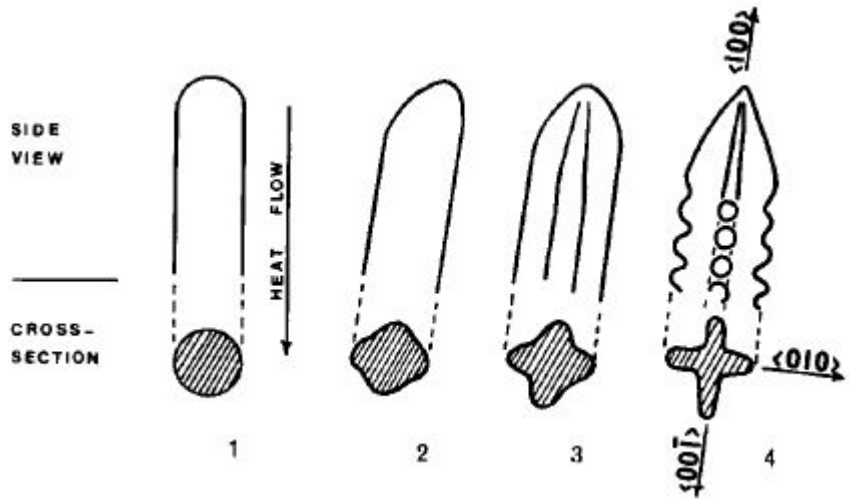

Fig. 1.13 : Sketch of the changing shape of the growth structure as the growth velocity is increased (Morris and Winegard, 1960). (1) Regular cell growing at low velocity; (2) regular cell growing in <100>dendrite direction; (3) flanged cell; (4) dendrite exhibiting the start of periodic lateral branching.

1.8 Hardness

Hardness is a measure of a material's resistance to localized plastic deformation. Early tests were based on natural minerals with a scale constructed solely on the ability of one material to scratch another that was softer. A qualitative and somewhat arbitrary hardness indexing scheme was devised, termed the Mohs scale, which ranged from 1 on the soft end for talc to 10 for diamond. Quantitative hardness techniques have been developed over the years in which a small indenter is forced into the surface of a material to be tested, under controlled conditions of load and rate of application. The depth or size of the resulting indentation is measured, which in turn is related to a hardness number; the softer material, the larger and deeper is the indentation, and the lower the hardness index number. There are several hardness test techniques such as Brinell, Vickers microhardness, Knoop microhardness, Rockwell and superficial Rockwell hardness test (Callister, 2006).

For Knoop and Vickers test a very small diamond indenter having pyramidal geometry is forced into the surface of the specimen. Applied loads are much smaller than for Rockwell and Brinell, ranging between 1 and 1000 g. The resulting impression is observed under a microscope and measured; this measurement is then converted into a hardness number. Careful specimen surface preparation may be necessary to ensure a well-defined indentation that may be accurately measured. The Knoop and Vickers hardness numbers are designated by HK and HV, respectively (Callister, 2006).

1.9 Dissipative Particle Dynamics

Dissipative particle dynamics (DPD) is a technique for simulating fluids from the mesoscale (10-100 nm and 10-100 ns) to the continuum limit. It was first introduced by Hoogerbrugge and Koelman and is based on the simulation of soft spheres, whose motion is governed by certain collision rules (Hoogerbrugge and Koelman, 1992; Koelman and Hoogerbrugge, 1993). DPD was improved most notably by Español and Warren (1995) and then by Groot and Warren (1997) and Pagonabarraga and Frenkel (2001) who introduced a density dependent conservative force into the algorithm. Recently a new parametrization method for DPD conservative forces was suggested by Travis, Bankhead, Good and Owens

(2007). This new scheme widens the realm of applicability by first removing the restriction of equal repulsive interactions between like beads, and second, by relating all conservative interactions between beads directly to cohesive energy densities.

A system of beads interact with each other as a result of pairwise additive forces comprising of conservative forces $\boldsymbol{F}^{\mathrm{C}}$, dissipative forces $\boldsymbol{F}^{\mathrm{D}}$, and random forces $\boldsymbol{F}^{\mathrm{R}}$,

$$\boldsymbol{F}_i = \sum_{j \neq i} \left(\boldsymbol{F}_{ij}^{C} + \boldsymbol{F}_{ij}^{D} + \boldsymbol{F}_{ij}^{R} \right) \tag{1.31}$$

The conservative force is defined through

$$\boldsymbol{F}_{ij}^{C} = a_{ij} \omega^{C}(r_{ij}) \hat{\boldsymbol{r}}_{ij} \tag{1.32}$$

where a_{ij} is the repulsive force parameter between particle i and j, ω^{C} is the conservative weight function, $r_{ij} = \left| \boldsymbol{r}_i - \boldsymbol{r}_j \right|$ and $\hat{r}_{ij}$ is a unit vector in the direction of $\boldsymbol{r}_{ij}$. The weight function is typically a linear ramp giving rise to very soft repulsive forces.

The dissipative force depends on both the positions and relative velocities of the particles $\boldsymbol{v}_{ij}$ through

$$\boldsymbol{F}_{ij}^{D} = -\zeta \omega^{D}(r_{ij}) (\boldsymbol{v}_{ij} \cdot \hat{\boldsymbol{r}}_{ij}) \hat{\boldsymbol{r}}_{ij} \tag{1.33}$$

where ω^{D} is the dissipative weight function, $\boldsymbol{v}_{ij} = \boldsymbol{v}_i - \boldsymbol{v}_j$, and the coefficient ζ controls the strength of the dissipative force. The dissipative force models the

viscous drag on a particle due to the surrounding molecules of the fluid represented by the bead.

Random force can represent thermal noise and it has defined

$$\boldsymbol{F}_{ij}^{R} = \sigma^{R}\omega^{R}(r_{ij})\xi_{ij}\Delta t^{-1/2}\hat{\boldsymbol{r}}_{ij} \tag{1.34}$$

where σ^{R} is a parameter that determines the magnitude of the random pair force between the particles, ω^{R} is the random force weight function, ξ_{ij} is a Gaussian distributed random variable, and Δt is the integration time step.

The combination of random and dissipative forces acts as a thermostat in DPD. The random force term tends to heat the system up, while the dissipative term damps out any increase in temperature.

1.10 Summary

Traditional casting usually solidifies one homogenous liquid by removing heat from liquid surface and it is solely dependent on the heat removal rate for the given alloy composition. Comparing conventional casting method, a novel scheme for refinement of alloy microstructure during casting is introduced. The process is realized by the creation of two liquids of alloy with an average composition which is the desired value but one freezes at a low temperature and the other at a high temperature. The two liquids are poured into the same casting mould simultaneously for mixing and solidification. Given that heat transfer is orders of magnitude faster than solute transport, it results in high-freezing temperature liquid being enormously supercooled. This will stimulate nucleation of solids and fluid mixing effect forced to spread these nuclei to entire material before finishing solidification. By these effects, greatly refined microstructure is expected and this idea has been validated by theoretical and experimental observation especially with Sn-Pb casting.

Ⅱ. Experiments

2.1 Alloy Production

The method of simultaneous casting with the aim of structural refinement was introduced in chapter 1. Experiments are needed to validate the concept. This technique involves handling two liquids and hence is difficult to implement in the laboratory when dealing with steel which has a very high melting temperature. It was decided therefore that the first stage would be performed using Sn and Pb. The corresponding phase diagram is shown in Fig. 2.1, which shows a maximum temperature just over 300 C, making it relatively easy to handle the melt. However, care must be exercised with respect to any toxic vapour properties.

It was required to make two kinds of alloy for comparing the microstructures made by conventional one-liquid casting and the new two-liquid casting method. Alloy 1 was made by traditional one-liquid casting and Alloy 2 was made by the two-liquid casting method. The chemical compositions of each liquid and the casting temperatures are listed in Table 2.1.

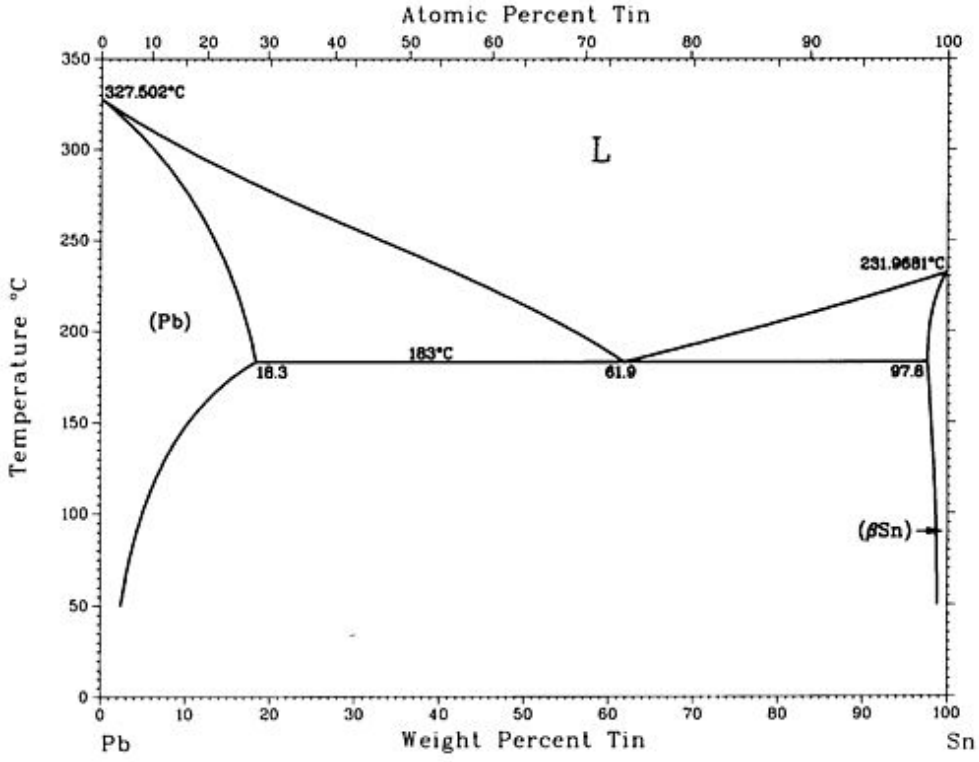

Fig. 2.1: Phase diagram of Sn and Pb binary alloy (Karakaya and Thompson, 1988).

		Mass / g	Sn / wt%	Pb / wt%	Casting Temperature / °C
Alloy 1	Liquid	125.75	80.02	19.98	240
Alloy 2	Liquid 1	61.19	100	0	240
	Liquid 2	61.40	60	40	200

Table 2.1: The compositions and casting temperatures of liquids of Alloy 1 and 2.

For preparing Alloy 1, a liquid which has total mass 125.75 g with 80.02 wt% Sn and 19.98 wt% Pb was casted at 240 °C. To make Alloy 2, two liquid was prepared. The chemical composition and total mass of Liquid 1 were 100 wt% Sn and 61.19 g and Liquid 1 was kept in temperature 240 °C. The chemical composition and total mass of Liquid 2 were 60 wt% Sn and 40 wt% Pb and 61.40 g and Liquid 2 was kept in temperature 200 °C. After preparing these two liquids, they were poured into a same mould simultaneously and then solidified.

2.2 Optical Microscopy

To prove the effect of two-liquid casting, it is necessary to compare the microstructures of Alloys 1 and 2. Samples were cold mounted and then polished using SiC paper and diamond suspension. For optical microscopy they were etched using solution of 100 mL distilled water, 25 mL nitric acid 65 % and 16 mL glacial acetic acid, for 10 s ~ 60 s (Günter Petzow, 1999).

2.3 Hardness Test

Vickers hardness tests were carried out with a load of 100 g for 10 s duration.

2.4 Energy Dispersive Spectroscopy

Measuring weight composition of grains and eutectic region of samples is required to understand more deeply about the mixing and solidification mechanism. Composition was measured using energy dispersive spectroscopy (EDS) on a *JEOL JSM-5900* scanning electron microscope. Samples were prepared as a same method with optical microscopy except with deeper etching.

2.5 X-ray Diffraction

Samples were prepared as a square shape which has 1 cm width and 1~2 mm height. They were polished using SiC paper and diamond suspension. They were analyzed by BRUKER D8 X-ray diffractometer. Beams were step scanned at speed of 0.2 degree per minute using Cu K_{α} X-rays.

Ⅲ. Results and Discussions

3.1 Optical Microscopy

3.1.1 One-Liquid Casting

Microstructures of the alloy made by one-liquid casting were observed using optical microscopy. Fig. 3.1 is from the chilled zone, Fig. 3.2 illustrates the columnar zone and Fig. 3.3 the equiaxed zone.

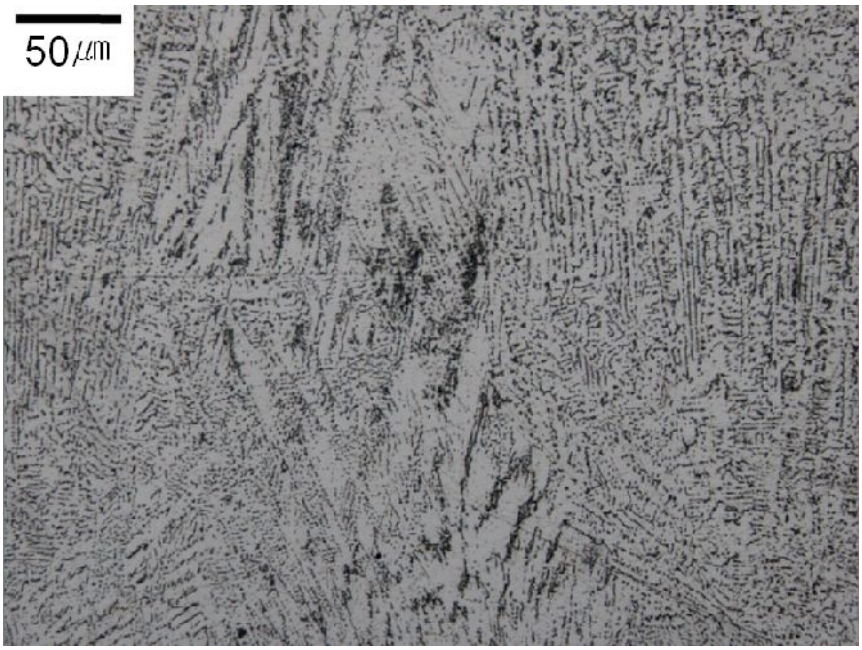

Fig. 3.1: Optical micrograph of chilled zone. One-liquid casting.

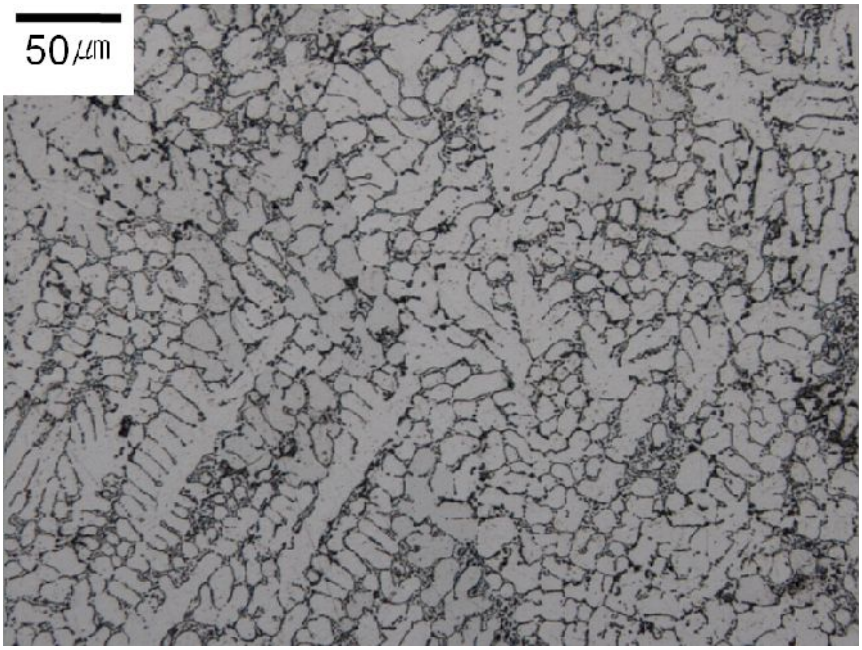

Fig. 3.2: Optical micrograph of columnar zone. One-liquid casting.

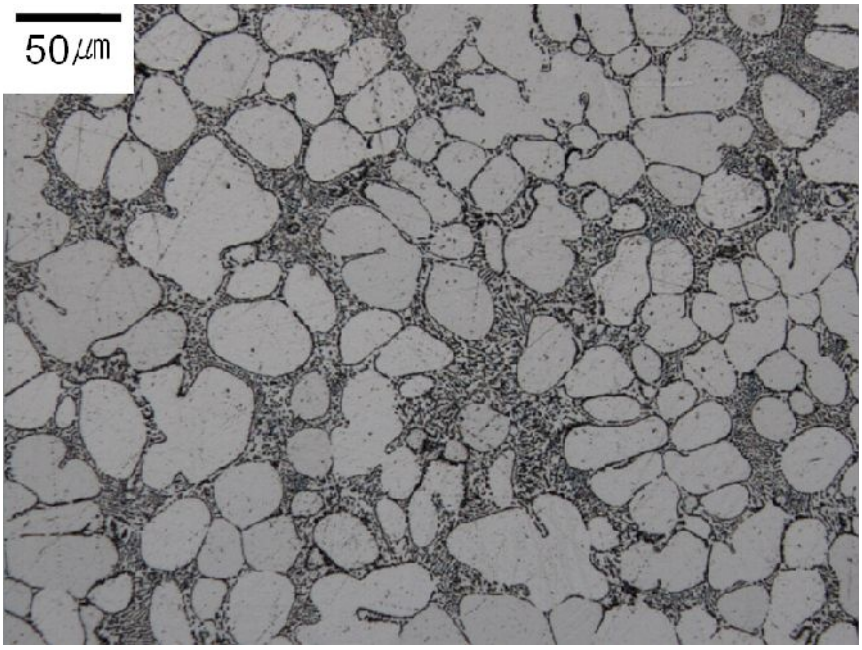

Fig. 3.3: Optical micrograph of equiaxed zone. One-liquid casting.

3.1.2 Two-Liquid Casting

The corresponding microstructures of the alloy made by simultaneously casting two different liquids are shown in Figs. 3.4-3.6, for the chilled, columnar and equiaxed zones respectively.

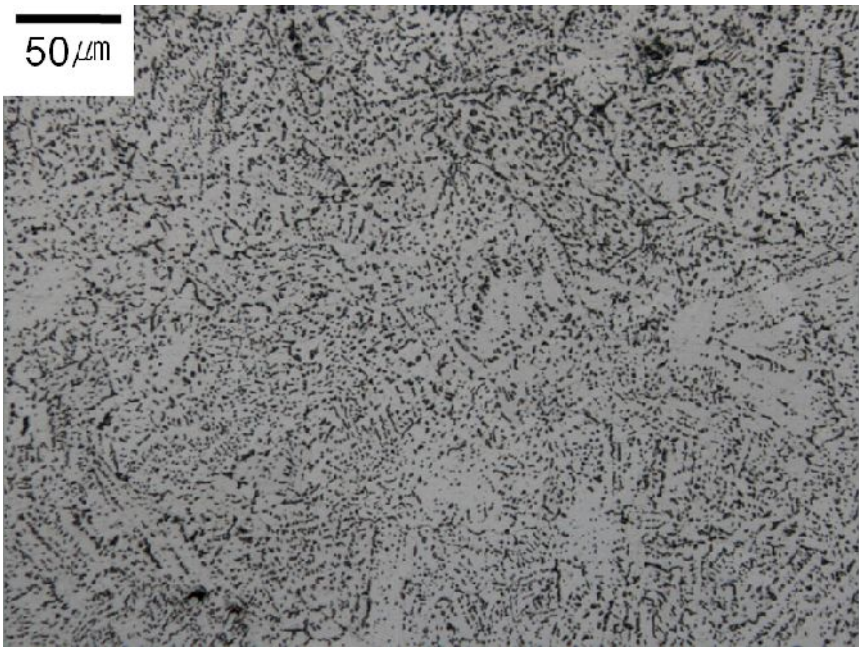

Fig. 3.4: Optical micrograph of chilled zone. Two-liquid casting.

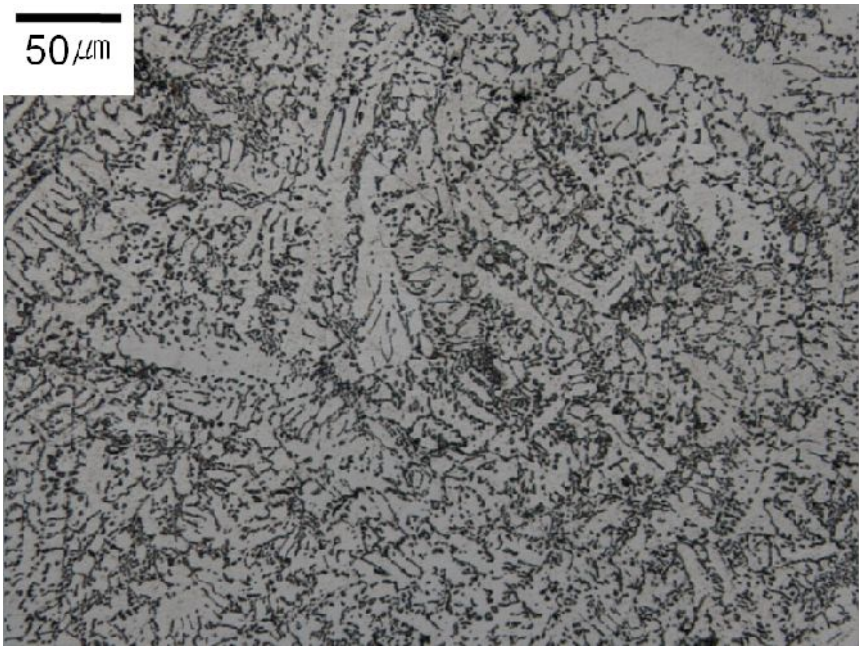

Fig. 3.5: Optical micrograph of columnar zone. Two-liquid casting.

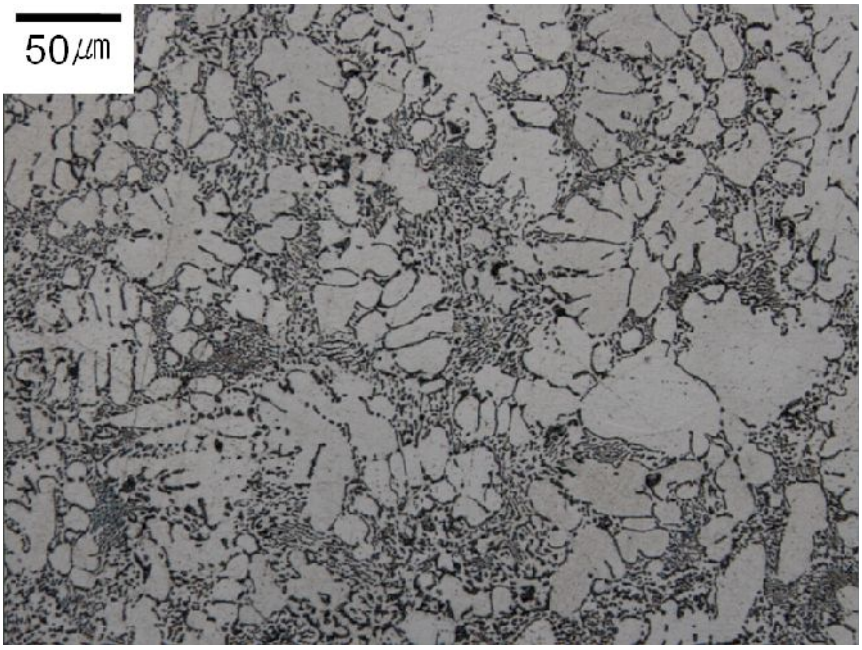

Fig. 3.6: Optical micrograph of equiaxed zone. Two-liquid casting.

3.1.3 Discussions

In the one-liquid casting, the chilled, columnar and equiaxed zones are easily resolved using optical microscopy. This is not the case in two-liquid casting. Quantitative data are discussed later in the text. The extent and distribution of the different zones is also different for the single and two-liquid castings. In the latter case, the width of the columnar region is much smaller than with the one-liquid casting, and there exists a bigger region which is a mixture of columnar and equiaxed microstructures. Even within the equiaxed zone, several small, radial dendrites are observed. This could represent evidence of the supercooling effect of the two-liquid casting process. The presumably nonuniform temperature distribution and supercooling effect in the two-liquid process, fractal grains and small dendrites are found between those which are equiaxed.

As expected, all alloys show primary Sn dendrites with interdendritic Sn-Pb eutectic. An important point is that the process of pouring liquid metal from one crucible to another during solidification can influence the morphology of primary Sn grains (Fan, 2002). The flow causes more spherical or rosette-like Sn dendrites, as described in semi-solid metal processing literature (Ji and Fan, 2002). However, in the current work, both alloys went through same pouring procedures and hence comparisons between the two alloys are justified.

Microstructure comparison between the one and two-liquid castings are focused on the equiaxed zone. Fig. 3.3 represents the equiaxed zone of one-liquid casting and the dendrites of Sn have smooth surfaces clearly separated from the eutectic. Fig. 3.6, which shows a radically different microstructure in the equiaxed zone of the two-liquid casting when compared with the normal process. The dendrites not only show greater branching but have rough surfaces and there is clear refinement of the microstructure.

Mean lineal intercept values, $\bar{L}$ were measured for the two types of castings and their values are listed in Table 3.1. The intercept is measured by imposing test lines onto the microstructure and counting the number of cross between the lines and grain boundaries.

Alloy	mean lineal intercept, $\bar{L}\ /\mu m$	Standard Deviation
Alloy 1	25	3.4
Alloy 2	13	2.2

Table 3.1: Mean lineal intercept and standard deviation of Alloy 1 and 2.

By comparing the optical micrographs and mean lineal intercepts, it is obvious that supercooling is achieved in the two-liquid process and that the microstructure has been significantly refined.

3.2 Microhardness Tests

Microhardness data are shown in Fig. 3.7, Table 3.2 and Table 3.3 and show that the two-liquid casting is in general slightly but significantly harder, consistent with its finer microstructure. Indentation is done on small grains in equiaxed zone of samples.

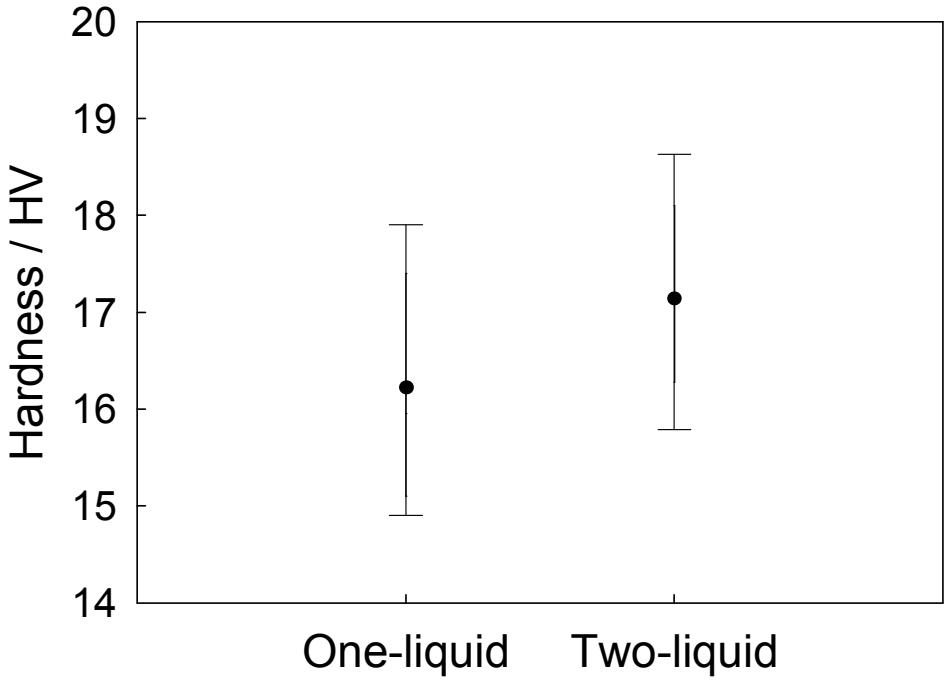

Fig. 3.7: Vickers hardness data measured using a 100 g load. Hardness values of the alloys made by one liquid casting and two liquid casting are illustrated.

Attempts	One-liquid / HV	Two-liquid / HV
1	14.9	16
2	16.2	16.8
3	15.9	17.2
4	17.4	16.3
5	17.9	18.2
6	18.3	15.3
7	15.4	16.3
8	16.5	17
9	15.2	17.7
10	15.5	16.5
11	14.9	18.1
12	16	18.7
13	15.4	15.2
14	15.9	18
15	16.5	16.2
16	17.3	17.5
17	14.6	18.1
18	17.8	16.4
19	17.9	18
20	17.4	16.1
21	17.5	18.1

22	17.2	18.6
23	15.1	18.8
24	15.1	17.5
25	14.9	17
26	15.1	16.1

Table 3.2: Vickers hardness data measured using a 100 g load. Indentation is done on small grains in equiaxed zone of samples.

Alloy	Microhardness / HV	Standard Deviation
Alloy 1	16.2	1.1
Alloy 2	17.1	1.0

Table 3.3: Mean Vickers hardness data and standard deviation measured using a 100 g load.

3.3 Energy Dispersive Spectroscopy

Energy dispersive spectroscopy (EDS) has been used to measure the compositions of the dendrites and eutectic regions of each sample. JSM-5900 machine is internally adopted ZAF errors correction function. The results are illustrated in Figs 3.8-3.9 for the dendrites of one-liquid casting and Figs. 3.10-3.11 for the eutectic

regions of two liquid casting. In the former case, the Pb concentrations are measured to be 2.64 and 2.18 wt%. Figs 3.10 and 3.11 are measurements of eutectic regions in the one-liquid casting and the Pb concentrations were 25.04 and 24.28 wt%. This was not found to vary significantly when other eutectic regions were measured, Table 3.4. This is not surprising given the narrow solidification temperature range and the fact the one-liquid casting has a unique liquid composition.

	Weight %	Atomic %
Dendrites 1	2.64	1.53
Dendrites 2	2.18	1.26
Dendrites 3	3.13	1.81
Dendrites 4	4.52	2.64
Eutectic region 1	25.04	16.06
Eutectic region 2	24.28	15.52
Eutectic region 3	24.01	15.33
Eutectic region 4	23.20	14.69

Table 3.4: Pb concentration in wt% and atomic% of dendrites and eutectic region is measured by EDS.

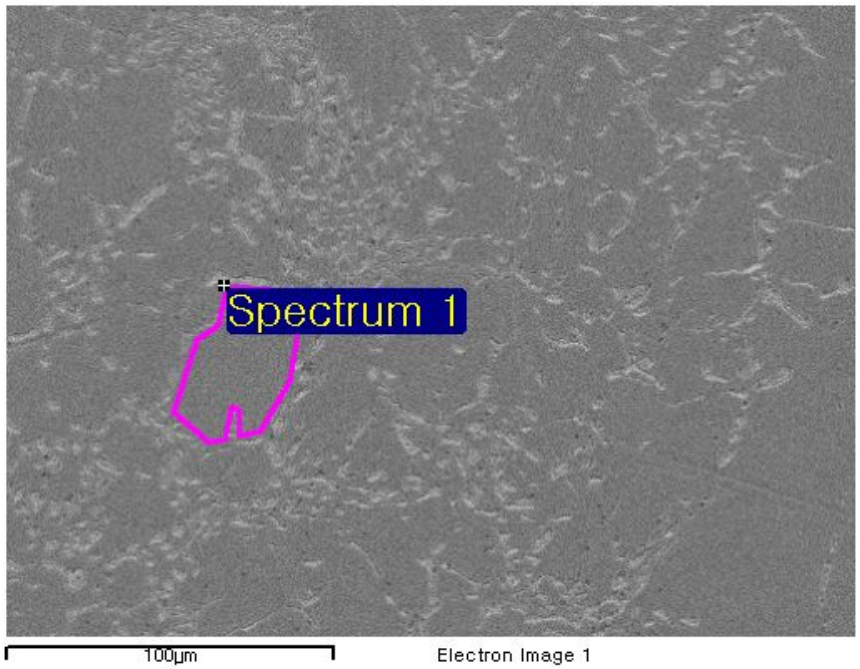

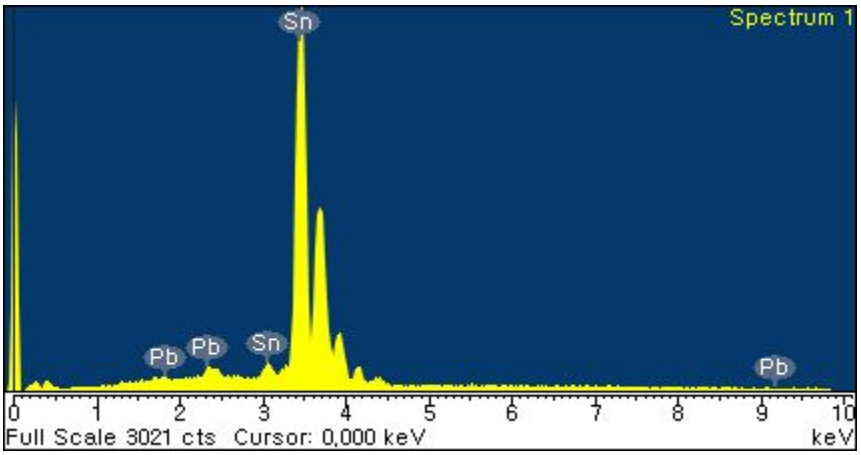

Element	Weight%	Atomic%
Sn L	97.36	98.47
Pb M	2.64	1.53
Totals	100.00	

Fig. 3.8: Concentration in wt% of marked grain area made by one-liquid casting.

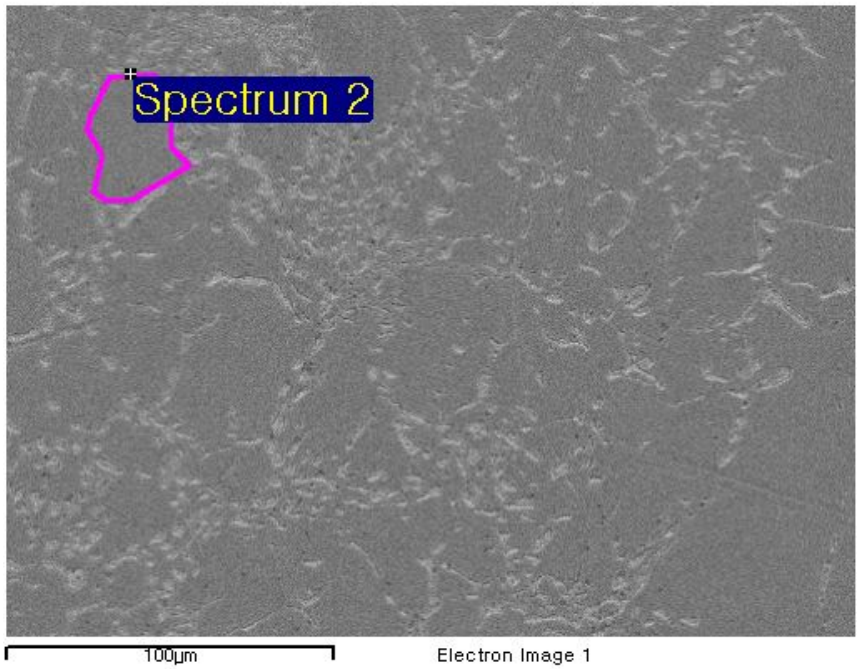

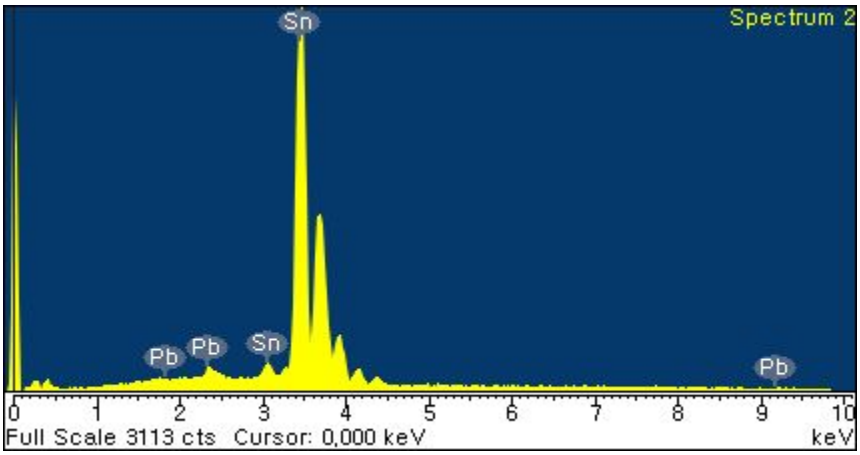

Element	Weight%	Atomic%
Sn L	97.82	98.74
Pb M	2.18	1.26
Totals	100.00	

Fig. 3.9: Concentration in wt% of marked grain area made by one-liquid casting.

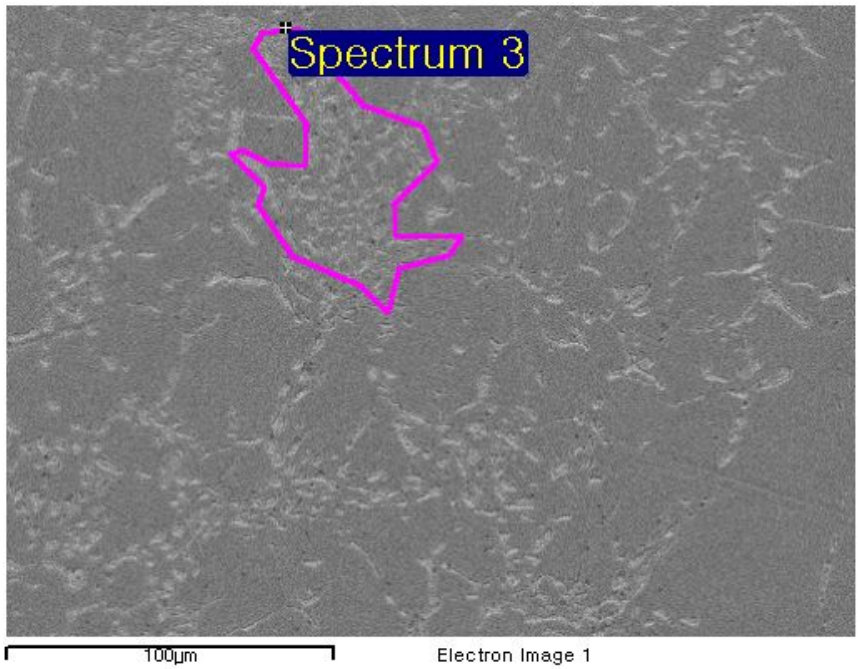

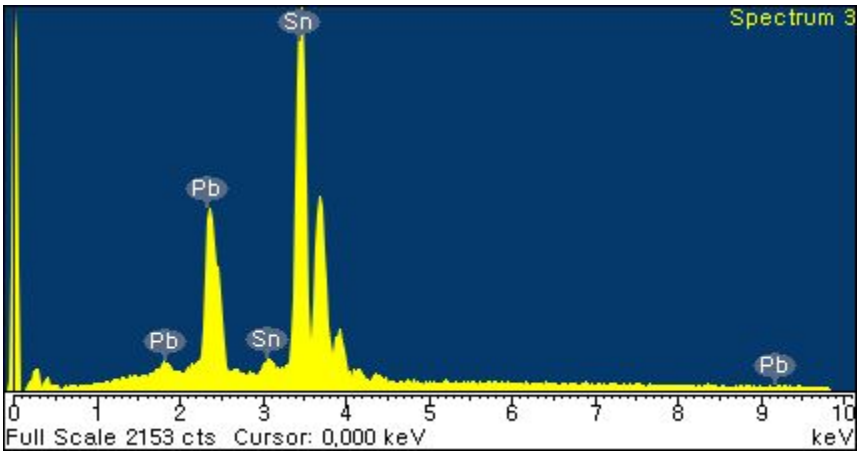

Element	Weight%	Atomic%
Sn L	74.96	83.94
Pb M	25.04	16.06
Totals	100.00	

Fig. 3.10: Concentration in wt% of marked eutectic region, one-liquid casting.

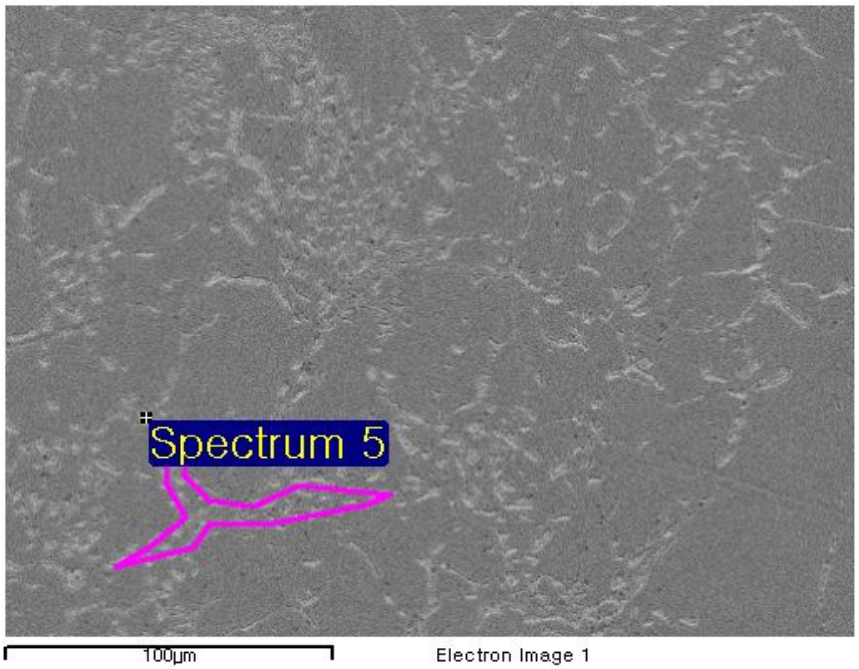

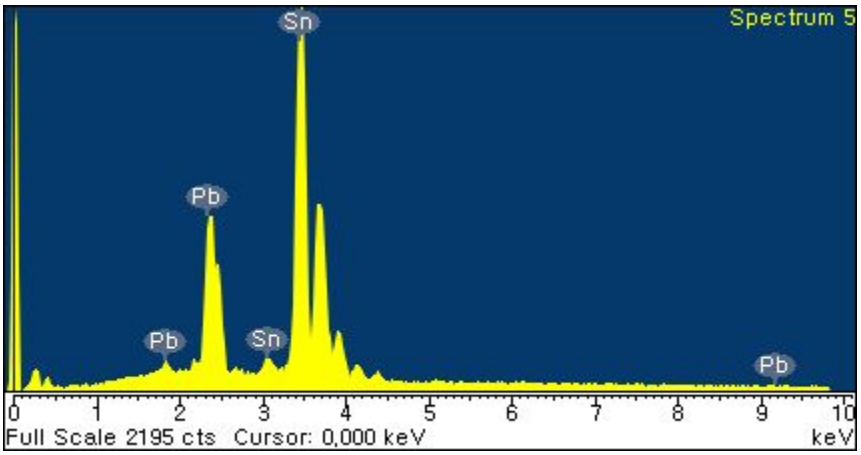

Element	Weight%	Atomic%
Sn L	75.72	84.48
Pb M	24.28	15.52
Totals	100.00	

Fig. 3.11: Concentration in wt% of marked eutectic region, one-liquid casting.

Figs 3.12 and 3.13 are measurements of marked dendrite area in the two-liquid casting and the concentration of Sn was found to be 100 wt%. During two-liquid casting, high liquidus-temperature and low liquidus-temperature fluids are mixed so that the former becomes supercooled and hence has an enhanced nucleation rate. In present work, chemical composition of the high temperature liquid is pure Sn so tin nuclei are first created by supercooling effect and are dispersed into the entire liquid by the mixing of fluids. That is the why dendrites of pure Sn are seen dispersed in the microstructure. The results show that the desired supercooling effect has been achieved before the two liquids become homogeneously mixed and of uniform composition.

Figs 3.14 and 3.15 are measurements of the eutectic regions in the two-liquid casting with Pb concentrations of 21.54 and 22.33 wt%. The Pb compositions of eutectic region by two-liquid casting were a little bit lower than the compositions by one-liquid casting. Fig. 3.16 was taken from one eutectic region by two-liquid casting and interesting result was found. In this picture, the concentration of Pb was 43.36 wt%, which is greater than that in either of the liquids used. There are two possible explanations of this observation; during the formation of the primary dendrites of Sn, the remaining liquid becomes enriched in Pb and hence the greater concentration of Pb in the eutectic regions. The second explanation depends on the non-equilibrium partitioning of Pb during dendrite precipitation. The correct interpretation is not yet resolved.

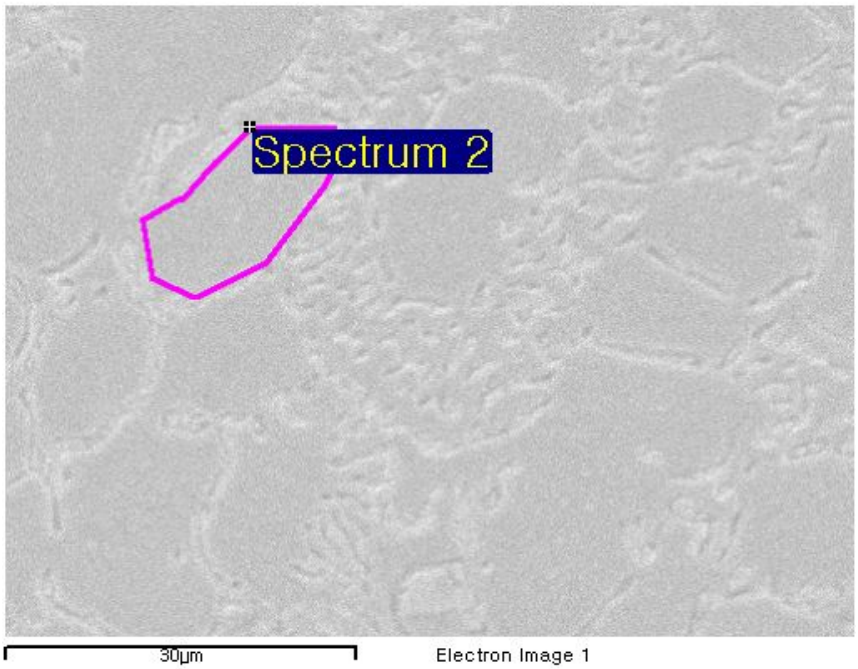

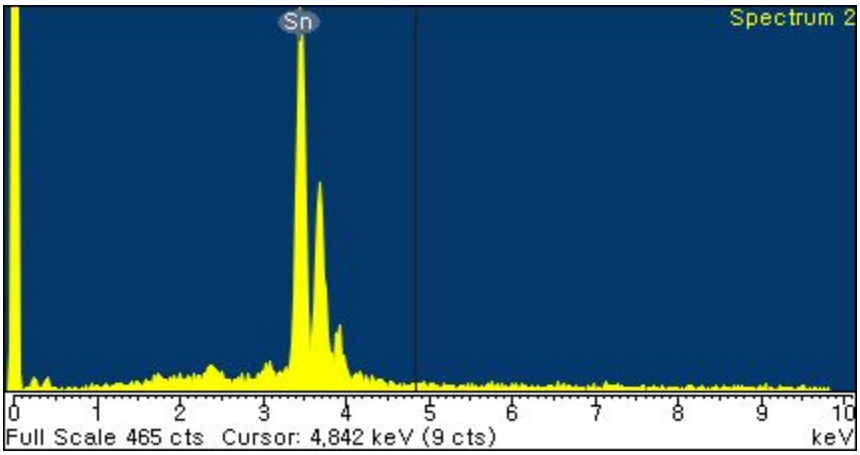

Element	Weight%	Atomic%
Sn L	100.00	100.00
Totals	100.00	

Fig. 3.12: Concentration in wt% of marked dendrite area, two-liquid casting.

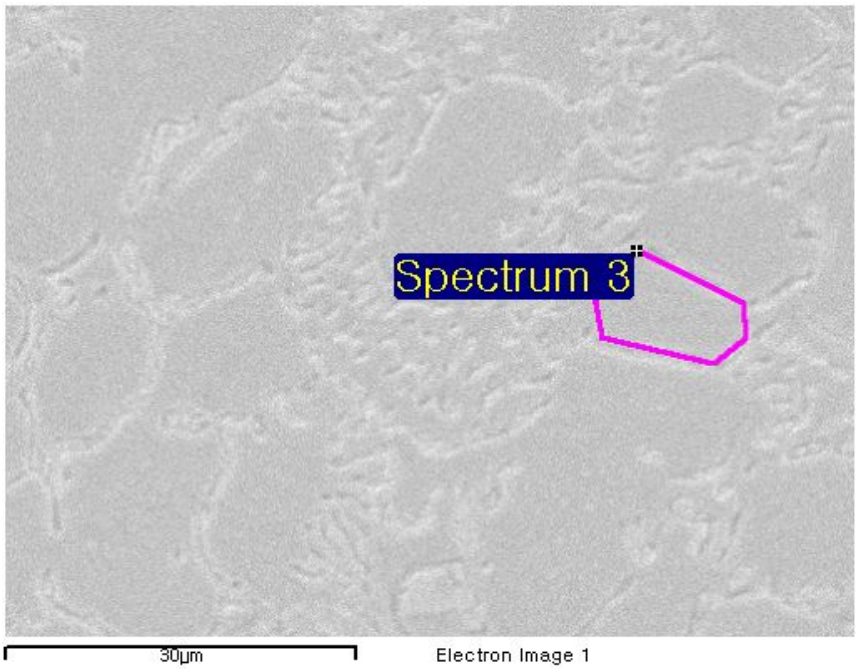

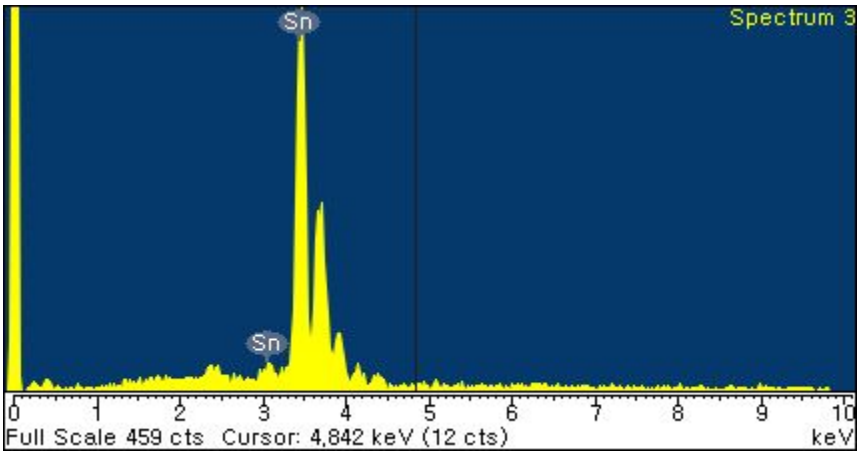

Element	Weight%	Atomic%
Sn L	100.00	100.00
Totals	100.00	

Fig. 3.13: Concentration in wt% of marked dendrite area, two-liquid casting.

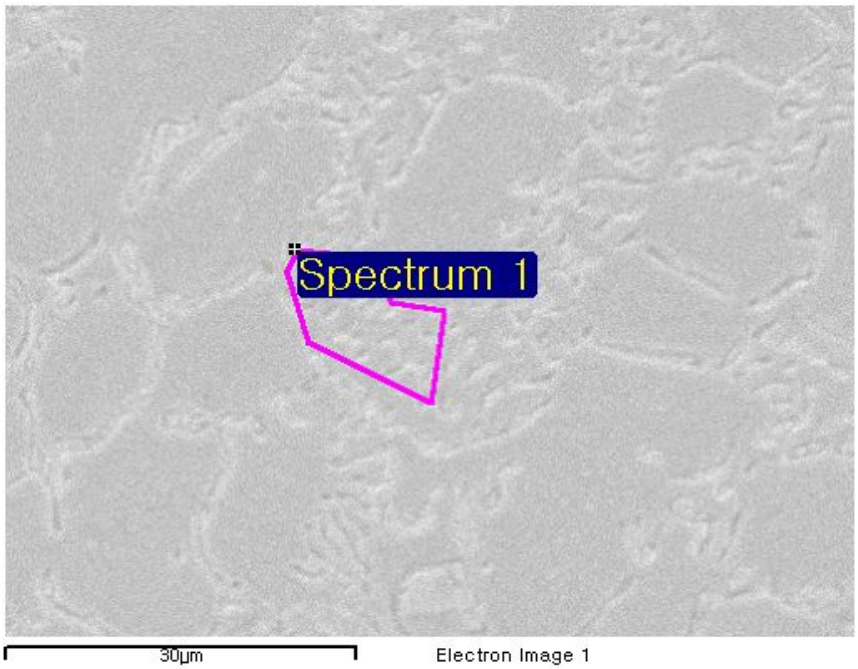

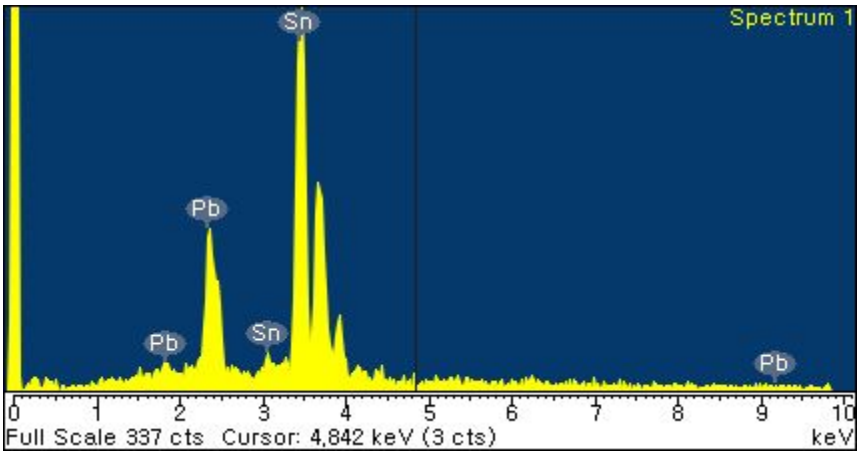

Element	Weight%	Atomic%
Sn L	78.46	86.41
Pb M	21.54	13.59
Totals	100.00	

Fig. 3.14: Concentration in wt% of marked eutectic region, two-liquid casting.

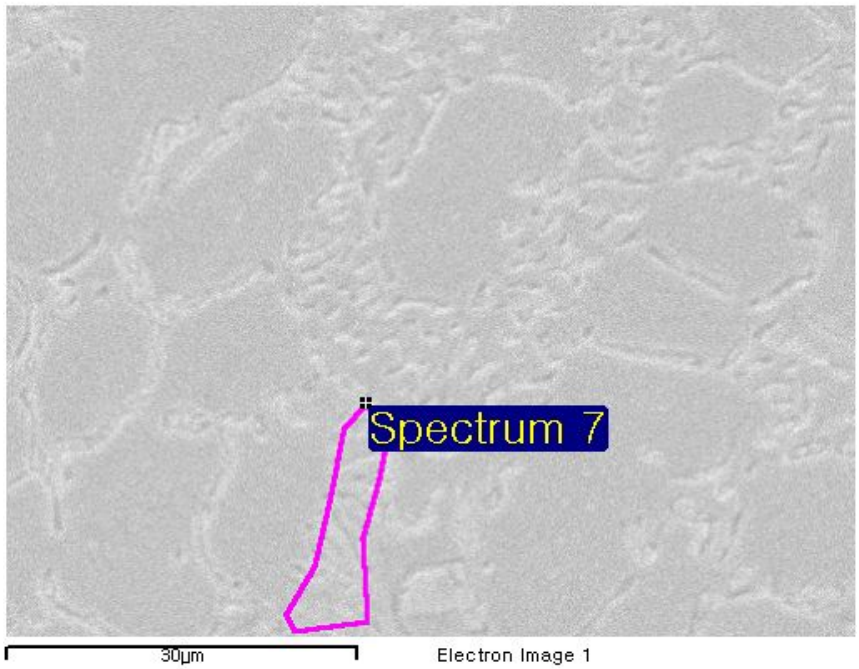

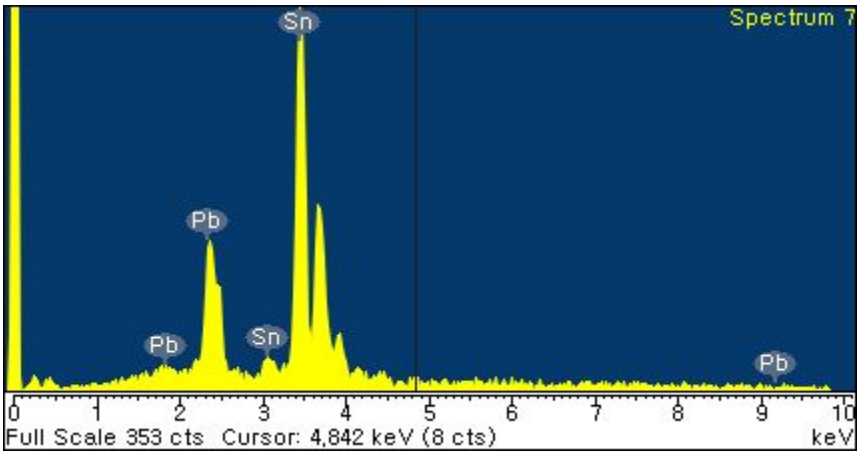

Element	Weight%	Atomic%
Sn L	77.67	85.86
Pb M	22.33	14.14
Totals	100.00	

Fig. 3.15: Concentration in wt% of marked eutectic region, two-liquid casting.

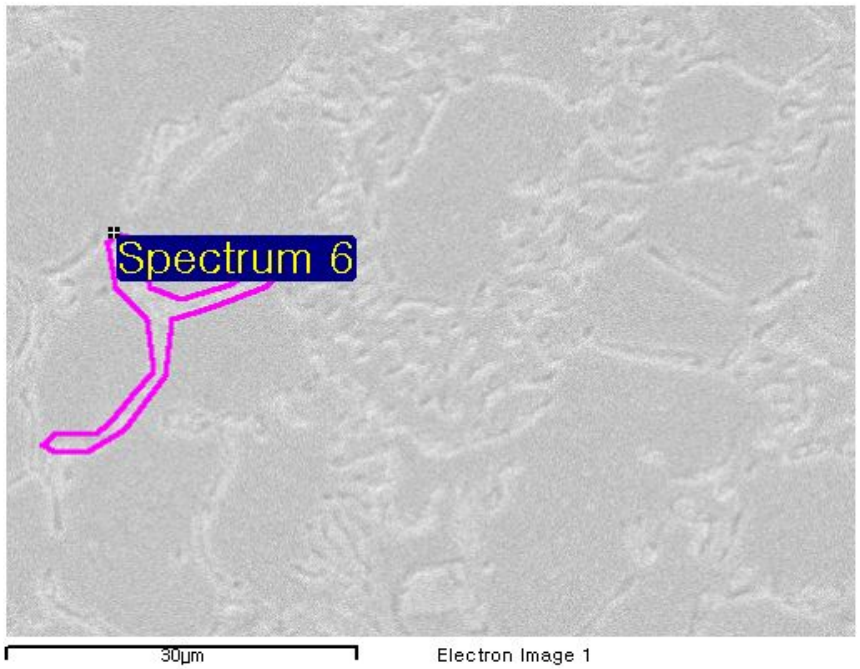

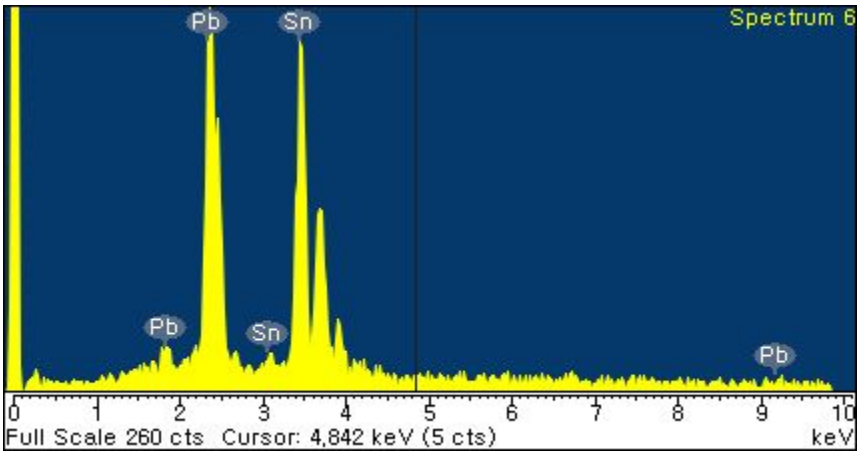

Element	Weight%	Atomic%
Sn L	56.64	69.51
Pb M	43.36	30.49
Totals	100.00	

Fig. 3.16: Concentration in wt% of marked region, two-liquid casting.

3.4 X-ray Diffraction

X-ray diffraction data of Pb and Sn are listed in Tables 3.3 and 3.4 (Hanawalt et al., 1938).

2θ	I	h	k	l	Comment
31.362	100	1	1	1	Strongest line
36.343	50	2	0	0	
52.553	50	2	2	0	
62.260	50	3	1	1	
65.186	17	2	2	2	
85.950	17	3	3	1	
87.889	17	4	2	0	

Table 3.5: X-ray diffraction data of Pb by Hanawalt et al., (1938)

2θ	I	h	k	l	Comment
30.699	100	2	0	0	Strongest line
32.054	80	1	0	1	
44.142	32	2	2	0	
45.068	80	2	1	1	

55.660	24	3	0	1
62.728	24	1	1	2
64.179	20	4	0	0
72.675	16	4	2	0
79.870	20	3	1	2
89.934	11	4	3	1
95.577	8	1	0	3
98.085	6	5	2	1
103.630	3	2	1	3
111.845	6	3	0	3
119.881	2	3	2	3
129.980	3	4	1	3
143.974	2	6	4	0

Table 3.6: X-ray diffraction data of Sn by Hanawalt et al., (1938)

The results from X-ray diffraction measurements on the two castings are presented in Fig. 3.17. In the two-liquid casting, the peak intensities for 2θ values at 31.36 and 52.28 which are from Pb are higher but the overall distribution of intensities is reasonable.

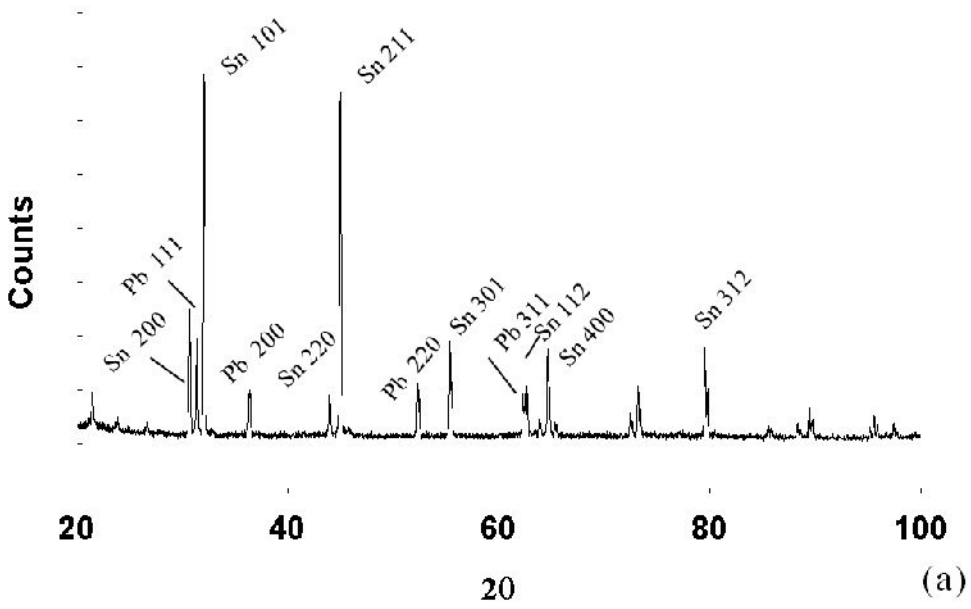

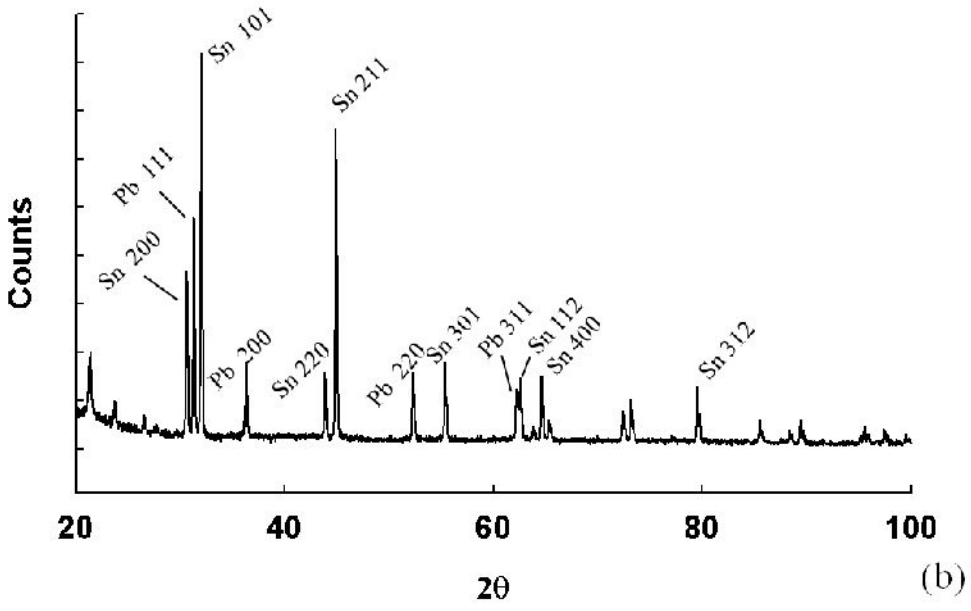

Fig. 3.17: X–ray diffraction patterns taken using CuKα radiation. Samples were prepared from (a) alloy of one-liquid casting, (b) alloy of two-liquid casting.

3.5 Discussions

During the simultaneous pouring of two different liquids, heat transfer from the hotter to the colder fluid, and mass transfer from the more concentrated liquid occurs. However, the heat transfer rate is expected to be an order of magnitude higher than that for mass transfer, permitting supercooling to be achieved for the high liquidus-temperature melt.

It is useful to imagine two extreme scenarios. First, because of the fast mixing effect, if the liquids homogenise prior to the achievement of supercooling, then the two-liquid casting must be identical to the normal process since the average composition of the two liquids used is equivalent to that of the single-liquid process. Second, if the solidification rate is too fast to spread the nuclei induced in the high liquidus-temperature fluid by supercooling then the final microstructure should be nonuniform. Therefore, the relation between solidification rate and mixing rate must be an important factor.

It has been verified in the present work that the microstructure is definitely refined and the hardness slightly increased by using the simultaneous casting process. This novel concept of two-liquid casting therefore allows the refinement of microstructure but there are unsolved problems such as high the high Pb concentration observed in some eutectic regions.

It is particularly interesting that the Sn concentration in the primary dendrites in the one-liquid casting was around 97 whereas the dendrites were almost pure Sn in the two-liquid casting. If the grain sizes were big and grains distribution nonuniform with clustering of the pure Sn dendrites then it could be argued that this new technique is not effective. However, the contrary was observed with many small, primary Sn primary dendrites which are a clear reflection of the supercooling effect inherent in the two-liquid casting technique.

Another possible manipulation by this technique could be phase selection. By careful selection of two liquids, it should be possible to choose the phases that grow and the sequence in which they form. For example, if any phase is preferred then by making a liquid that can solidify to that phase it should be possible to alter the solidification microstructure.

3.6 Summary

Using both qualitative and quantitative observations based on optical microscopy, it has been demonstrated that the two-liquid casting is effective in refining the overall microstructure. In the present case, the hardness only changed slightly, but it is possible to imagine iron-based systems where the consequences could be greater. A most interesting outcome is that the compositions of the primary dendrites are quite different in the one and two-liquid castings, providing further strong evidence of the postulated supercooling inherent in the simultaneous casting process.

Ⅳ. Summary and Future work

4.1 Summary

The aim of this work was to introduce a novel concept that can refine the microstructure of alloy during casting. Rather than casting a single, homogeneous liquid of the intended composition, two such liquids with an average composition which is that desired, are simultaneously cast. Their compositions are chosen so that one of the two has a liquidus temperature which is lower than that of the other. Heat and mass transfer occurs at the interface between the two liquids during the process of pouring into the mould. Since heat transfer is much faster than that of mass, a constitutionally supercooled layer is established and many nuclei of the solid phase stimulated. Subsequent mixing disperses the nuclei apparently uniformly throughout the melt. In this method heat removal occurs not only the interface between mould wall and liquids but also at the interface between the component liquids. The method can therefore be applied to bulk production whereas supercooling techniques associated with the casting of single liquids are not suitable for bulk production.

Several experiments were performed using a model alloy-system to validate the concept. The results confirm the general principles with clear evidence that the

simultaneous casting of two appropriately chosen liquids leads to structural refinement, as quantified using mean lineal intercept and hardness measurements. There are some interesting observations of the apparently uniform dispersion of almost pure Sn dendrites within the microstructure, proving not only the supercooling effect, but also the mixing that follows the initial supercooling at the interfaces between the liquid streams. There are some unexplained observations, such as the concentration of Pb in the eutectic regions.

4.2 Future Work

It is possible in principle to use the simultaneous casting method to induce deliberately, metastable phases which are not possible during single liquid casting. For example, it is known that ferritic stainless steels can be induced to solidify into an austenitic structure by seeding the melt with austenite. The present work suggests an alternative and perhaps more effective way of doing this.

It would be useful to simulate the process mathematically, in order to gain insight into the detailed phenomena at the liquid-liquid interfaces and to study the roles of streamlined versus turbulent mixing. Such simulations could be conducted using a method known as dissipative particle dynamics.

Finally, although the experiments here have been conducted on a model system based on Pb and Sn, the ultimate intention is to apply it to iron alloys. The trouble is that this requires much more sophisticated equipment because of the high melting temperatures involved. Further work will therefore depend on investment in this area.

Ⅴ. References

Hall, E.O. : The deformation and ageing of mild steel: III. Discussion of results, *Proceedings of the Physical Society*, Vol. 64B, pp. 747-753, 1951

Petch, N.J. : The cleavage strength of polycrystals, *Journal of the Iron and Steel Institute,* Vol. 174, pp 25-28, 1953

Greer, A. L. : Metallic glasses, *Science*, Vol. 267, pp. 1947-1953, 1995

Fan, Z. : Semisolid metal processing, *International Materials Reviews*, Vol. 47, pp. 49-85, 2002

S. Ji and Z. Fan : Solidification behavior of Sn-15 wt pct Pb alloy under a high shear rate and high intensity of turbulence during semisolid processing, *Metallurgical and Materials Transactions A*, Vol. 33, pp. 3511-3520, 2002

Campanella, T. Charbon, C. and M. Rappaz : Grain refinement induced by electromagnetic stirring: A dendrite fragmentation criterion, *Metallurgical and Materials Transactions A*, Vol. 35, pp. 3201-3210, 2004

Qin, R. S. and Zhou, B. L. : Effect of electric current pulses on grain size in castings, *International Journal of Non-equilibrium Processing*, Vol. 11, pp. 77-86, 1998

R.S Qin and E.R. Wallach : A phase-field model coupled with a thermodynamic database, *Acta Materialia*, Vol. 51, pp. 6199-6210, 2003

B. Vonnegut : Variation with temperature of the nucleation rate of supercooled liquid tin and water drops, *Journal of Colloid Science*, Vol. 3, pp. 563-569, 1948

H. S. Chen and D. Turnbull : The specific heat of tin and gallium in their stable and undercooled pure liquid states, *Acta Metallurgica*, Vol. 16, pp. 369-373, 1968

H. S. Chen and D. Turnbull : Thermal evidence of transition in gold-silicon-germanium alloy, *Applied Physics Letters*, Vol. 10, pp. 284-286, 1967

Nemchinsky, V. A. : Heat transfer in a liquid droplet hanging at the tip of an electrode during arc welding, *Journal of Physics D: Applied Physics*, Vol. 30, pp. 1120-1124, 1997

Fridberg, J. Torndahl, L. and Hillert, M. : Diffusion in iron, *Jernkontorets annaler*, Vol. 153, pp. 263-276, 1969

Beckermann, C. and Viskanta, R. : Modelling transport during alloy solidification, *Applied Mechanics Reviews*, Vol. 46, pp. 1-27, 1993

P. G. Enright, L. Katgerman, J. C. Ludwig and S. Rogers : Mixing and solidification of a turbulent liquid jet in a co-flowing stream, *International Journal for Numerical Methods in Engineering*, Vol. 24, Issue 1, pp. 231 – 249, 1987

S. Rogers, L. Katgerman, P.G. Enright and N.A. Darby : Modelling of liquid-liquid metal mixing, *Applied Scientific Research*, Vol. 44, pp. 175-195, 1987

Karl P. Travis, Mark Bankhead, Kevin Good and Scott L. Owens : New parametrization method for dissipative particle dynamics, *The Journal of Chemical Physics*, Vol. 127, 014109, 2007

L.R. Morris and W.C. Winegard : The cell to dendrite transition, *Journal of Crystal Growth*, Vol. 6, pp. 61-66, 1969

J. D. Hanawalt, H. W. Rinn and L. K. Frevel : Chemical Analysis by X-Ray Diffraction, *Industrial & Engineering Chemistry Analytical Edition*, Volume 10, Issue 9, pp 457–512, 1938

L. He and E. Ma : Processing and microhardness of bulk Cu-Fe nanocomposites, *Nanostructured Materials*, Vol. 7, Issue 3, pp. 327-339, 1996

J . Gil Sevillano and J . Aldazabal : Ductilization of nanocrystalline materials for structural applications, *Scripta Materialia*, Vol. 51 , Issue 8, pp 795 – 800, 2004

Flemings, M. C. : Solidification Processing, *McGraw-Hill*, 1974

R. V. Kumar : Heat and mass transfer, *Cambridge*

E.L. Cussler : "Diffusion. Mass Transfer in Fluid Systems", 2nd edition, *Cambridge University Press*, 1997.

William D. Callister : “Materials Science and Engineering: An Introduction”, 7th edition, Wiley, 2006

Acknowledgments

I would like to express my heartfelt thanks to my advisors, Professor Bhadeshia, H. K. D. H. and Professor Qin, Rongshan for their great encouragement, supports, and for insightful lectures and presentations. I would also like to thank to Professor Hae-Geon Lee, Professor In Gee Kim for their so much advices and supports.

I would like to express my thanks to all members in Computational Metallurgy Laboratory, for all their help and for all the memories we have.

I would like to record my deep sense of appreciation for all my family, especially my parents, for their everlasting love and devotion.

Finally, I would like to thank to my wife wholeheartedly and promise my eternal love.

CURRICULUM VITAE

Name: Kim, Yong Ki (金容基)

Date of birth: 9th July, 1979

Place of birth: Gyeong-ki province, South Korea

Address: 1-1502, Graduate Apt., POSTECH,
Hyoja-Dong, Nam-Gu, Pohang,
Kyungbuk, 790-784, South Korea

Education:

M. S. 2009, POSTECH (Pohang, Korea), Graduate Institute of Ferrous Technology, Computational Metallurgy.
B. S. 2007, POSTECH (Pohang, Korea), Department of Chemical Engineering